INVITED PAPER

Additively Manufactured RF Components and Modules: Toward Empowering the Birth of Cost-Efficient Dense and Ubiquitous IoT Implementations

This paper provides a review of inkjet printing and its application to a wide range of RF/microwave and sensing applications. Examples of inkjet-printed devices that are presented include RFID tags, energy-harvesting circuits, passive microwave interconnects and packaging, and carbon-nanotube-based gas sensors.

By Syed Abdullah Nauroze, *Student Member IEEE*, Jimmy G. Hester, *Student Member IEEE*, Bijan K. Tehrani, *Student Member IEEE*, Wenjing Su, *Student Member IEEE*, Jo Bito, *Student Member IEEE*, Ryan Bahr, *Student Member IEEE*, John Kimionis, *Student Member IEEE*, and Manos M. Tentzeris, *Fellow IEEE*

ABSTRACT | In this review, the particular importance and associated opportunities of additively manufactured radio-frequency (RF) components and modules for Internet of Things (IoT) and millimeter-wave ubiquitous sensing applications is thoroughly discussed. First, the current advances and capabilities of additive manufacturing (AM) tools are presented. Then, completely printed chipless radio-frequency identification (RFID) systems, and their current capabilities and limitations are reported. The focus is then shifted toward more complex backscattering energy autonomous RF structures. For each of the essential components of these structures, that encompass energy harvesting and storage, backscattering front ends, passive components, interconnects, packaging, shape-chaging (4-D printed) topologies and sensing elements, current trends are described and representative state-of-the-art examples reported. Finally, the results of this analysis are used to argue for the unique appeal of AM RF components and systems toward empowering a technological revolution of cost-efficient dense and ubiquitous IoT implementations.

Manuscript received November 16, 2016; revised December 20, 2016; accepted January 10, 2017.Date of publication February 24, 2017; date of current version March 20, 2017.

The authors are with the School of Electrical and Computer Engineering, Georgia Institute of Technology, Atlanta, GA 30332-250, U.S.A. (e-mail: nauroze@gatech.edu).

KEYWORDS | Additive manufacturing (AM); backscattering; encapsulation; energy harvesting; flexible electronics; flexible substrate integrated waveguide (SIW); inkjet-printed passive components; inkjet printing; interconnects; Internet of Things (IoT); microfluidics; multilayer structures; packaging; radio-frequency identification (RFID); smart skins; Van Atta array; via holes; 3-D printing

I. INTRODUCTION

The exponential growth in wireless and mobile communication technologies in the last decade has resulted in the integration of one or more communication modules in almost every object around us ranging from our cars, personal computers to inventory tracking systems for industry automation. This has motivated academia and industry to conduct a wide range of research and development to realize applications such as 5G, the Internet-of-things (IoT) and smart skins (SS) that interconnect different objects with sensing and processing capabilities which can communicate with each other at ultrahigh speeds without human interaction.

A ubiquitous adoption of such systems requires rapid prototyping techniques that are low cost, flexible, environmen-

Digital Object Identifier: 10.1109/JPROC.2017.2658565

tally friendly and can be easily scaled to large numbers. However, current lithography-based (subtractive) manufacturing technologies are expensive, produce harmful byproducts, and require longer prototype fabrication time, making them unsuitable to meet the demands of rapidly growing radio-frequency (RF) electronics and communication industry. That is why additive manufacturing technologies (AMTs) such as inkjet and 3-D printing have attracted notable attention in the past years especially in the field of flexible electronics due to their lower setup cost, high repeatability, wide scalability, and environmental benignity as compared to the traditional subtractive processes such as milling and lithography [1]–[3]. Moreover, the typical feature size of 1–20 μm and 10–50 μm can be achieved using inkjet-printing technology and 3-D-printing technology, respectively, making them ideal for realization of RF and millimeter-wave (mm-wave) applications such as IoT and SS.

AMTs involve the direct deposition of different materials in layer-by-layer fashion to form complex 3-D objects without wasting much or any material [4]–[6]. The two most prevalent AMTs used today are inkjet printing and 3-D printing. One of the key advantages of inkjet printing is the capability of direct deposition of a wide range of materials such as conductive, dielectric, and semiconductor inks on a variety of substrates including paper, glass, semiconductor wafers, and polymers [7]–[13]. Moreover, inkjet-printing technology can be used to easily realize a multilayer structure by depositing different types of inks for each layer. However, 3-D-printing technologies focus on the ability to print free-form 3-D objects, which conventional subtractive manufacturing tools cannot create, such as interior cavities and meshes that allow variations of dielectric constants both with and without support materials. Three-dimensional printing generally prints either dielectrics or conductors in a single printing process and seldom both *in situ*. Nevertheless, this AMT is expected to expand in the direction of simultaneous multimaterial printing.

Recent advances in additive manufacturing (AM) are very promising for the birth of fully printed low-cost RF nodes and motes for the IoT, including their possible integration into future fifth-generation (5G) networks. Furthermore, such progress is being achieved concurrently for two similar but very distinct radio-frequency identification (RFID)-based approaches that either include or not (chipless) the use of active electronics. After briefly describing the current state of the art in AM tools in Section II, the minimalist but quickly maturing approach of fully printed chipless RFIDs is described, and its current progress is reported in Section III. Then, focus is shifted to the more complex 3-D/inkjet-printed RF structures, such as backscattering energy-autonomous motes and, more specifically, to the current reports of efforts whose results are representative of a promising trend leading toward the birth of such fully additively manufactured RF systems. These essential RF components and elements include self-powering architectures, sensors and RF components, and modules in System-on-Package (SoP) implementations using AMTs. Section IV discusses different practical methods to allow wireless devices and sensors to be self-powered using ambient energy sources such as solar, RF, vibration, and heat. Section V shows key printed RF components used in mm-wave nodes that include fully inkjet-printed high-Q passive structures, multilayer flexible RF components along with techniques to realize on-package 2-D and 3-D fully printed RF interconnects along with state-of-the-art SoP solutions using AMT, which will constitute the backbone of the nodes' circuitry. Next, Section V-E presents the recent advances in novel inkjet-printed flexible sensors that enable the wireless nodes to detect changes in its environment and generate a corresponding response. Finally, Section VI concludes.

II. INKJET PRINTING TECHNOLOGIES

One of the key advantages of the traditional lithography-based (subtractive) processes is their ability to fabricate structures with extremely high resolution. Even though these manufacturing techniques continue to push the limits of Moore's law to realize smaller and faster devices, they are proving to be insufficient to meet the demands of future technologies due to their inability to fabricate rapid, low-cost, environment friendly flexible prototypes. For example, a traditional foundry uses different types of tools for sputtering, spin coating, masking to fabricate a single device, however, inkjet printing requires only a single printing tool to realize a design. This results in significant reduction in cost and lead time to fabricate a prototype. That is why AMTs such as inkjet printing have emerged as one of the key manufacturing techniques that are driving electronics and communication industries to realize the future generation of high-speed, low-cost, and environmentally friendly IoT, SS, and 5G nodes that can be rapidly fabricated and easily scaled to large numbers. Moreover, current piezoelectric-based inkjet printers can achieve feature size of 20 μm, which makes them ideal for RF integrated modules up to the mm-wave frequency range, especially in SoP implementations, which integrate multiple RF components by directly printing on the silicon substrate and package, thereby eliminating the need for external connections, effectively and drastically reducing the size, and increasing the efficiency of the overall device. Lower feature sizes (< 1 μm) can be achieved with electrohydrodynamic-based inkjet-printing systems, both experimental and commercial, however piezoelectric-based technology is of specific interest for the purpose of integration with existing large-scale tooling technology of the same piezoelectric mechanism [14].

A typical inkjet printer consists of one or more inkjet-printer heads that disposes the ink onto the substrate placed on top of a movable platform as shown in Fig. 1. The movement of the inkjet-printer head and the platform can be electrically controlled by a computer. Each inkjet-printer head houses an ink cartridge to store the ink and consists of an array of nozzles with individual piezoelectric elements. The ink goes from the cartridge into the nozzle via capillary effect and is dispensed in the form of droplets onto the target substrate in a Drop on Demand fashion, i.e., one or more nozzles are triggered by applying a voltage across

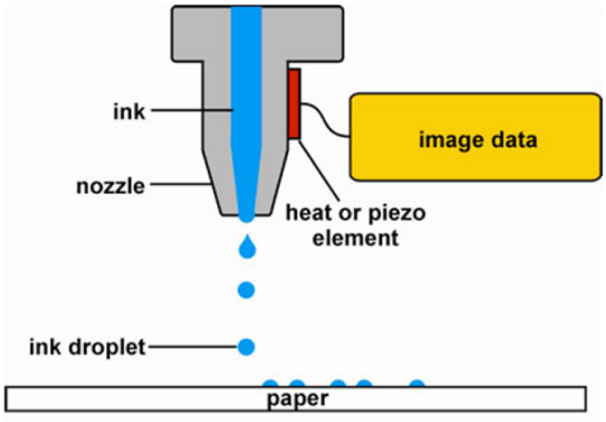

Fig. 1. ***Schematic of a typical inkjet printer head (image from http://www.dp3project.org/technologies/digital-printing/inkjet).***

the respective piezoelectric element to release droplets of ink according to the desired pattern. The volume of each droplet can vary from 1 to 10 pL depending on the type of cartridge.

Inks mainly comprise dielectric, conductive, or other active materials dispersed in a solvent, however, the choice of the solvent (e.g., water, ethanol) as well its composition depends on a number of factors including choice of dispersed material, target substrate, print head jetting ability, sintering conditions, etc. This gives inkjet printing a unique advantage for an *in situ* rapid fabrication of 3-D low-cost flexible prototypes with high resolution and reliability by directly printing a wide variety of inks on different types of substrates without any material waste or producing any harmful byproducts, which makes it extremely environmentally friendly as well.

Apart from the printing, the postprocessing and preprocessing of the inks on a given substrate is very important as well. Therefore, they have to be optimized to avoid spreading of the ink, they have to have good adhesion to the substrate or other printed layers, and they have to ensure good conductivity without breaking or destroying other components already in place. The optimization includes signal waveform shape for jetting, cartridge and platen temperature, drop spacing, ink viscosity, number of layers, sintering temperature, time, etc. For example, a commercially available silver nanoparticle (SNP) ink with an ethanol solvent requires around five layers of SNP ink on photopaper with sintering temperature of 120 °C for 1–2 h in vacuum oven to achieve bulk-level conductivity [9]. On the other hand, Diamine silver acetate (DSA) is a particle-free reactive silver ink that can be cured at mild temperatures (60 °C) but requires 10–15 layers of DSA ink to achieve bulk silver conductivity on photo paper substrates.

Table 1 outlines the processing parameters of four commonly used ink materials for inkjet printing, including silver nanoparticle dispersions, SU-8 polymer, PVP polymer, and CNT dispersions. The ability to pattern multiple materials with inkjet printing allows for the realization of multilayer electronic structures, such as passive components, vias, sensors, and fully printed RF substrates. In order to allow for efficient multilayer fabrication, several factors must be taken into consideration. First, pattern alignment must be performed through a fiducial system using alignment marks or features of the printed patterns. Second, the wettability of ink materials with printed films must be evaluated. This factor is typically evaluated through the comparison of the surface tension of the ink and the surface energy of the host substrate, either a bulk material or a previously printed pattern. In order to ensure proper wetting, a difference of 10 mN m^{-1} is desired between the surface tension of the ink and the surface energy of the accepting host [15]. The surface energy of both bulk substrates and inkjet-printed films is typically modified through the use of UV ozone and plasma treatments to ensure the integrity of multilayer structures.

III. CHIPLESS RFID CONFIGURATIONS FOR AM TAGS FOR IOT AND 5G APPLICATIONS

Recent decades have witnessed the wide adoption of RFID systems in various industries, such as manufacturing, supply-chain management, defense, and healthcare. Nevertheless, these tags require the use of an RFID integrated circuit (IC), which primarily determines the cost of each device, because of its intrinsic market cost as well as its expensive process of integration with the RFID antenna. In addition to their costs, these ICs need to be powered, which is achieved by the use of either a battery or an RF energy-harvesting scheme, which further increases costs, or imposes limitations on their real-world applicability (such as range limitations). In addressing the problems mentioned above, researchers have proposed various designs on the RFID tags with IC components removed: chipless RFID tags. Identification techniques such as barcode and QR code can be easily realized through the use of AMTs such as printing, and are thus commonly used in markets where RFIDs could otherwise dominate. However, chipless RFID, which can be fabricated by inkjet-printing technology [16]–[18], feature a competitive cost, a real-time encoding capability, a platform for various add-on applications such as sensing [16], [17] and localization [19], [20], and even a larger range [21]. Chipless RFID

Table 1 Processing Parameters of Different Inkjet-Printing Materials

	Standard Drop Spacing	Per-Layer Thickness	Thermal Curing	UV Cross-Linking	Sintering	Application
Silver Nanoparticle	20 μm	500–800 nm	100°C	No	< 200°C	Conductive patterns
SU-8 Polymer	20 μm	4–6 μm	100°C	Yes	No	Thick insulators/printed RF substrates
PVP Polymer	25 μm	300–500 nm	150°C	No	No	Thin dielectric films
CNT Dispersion	25 μm	10–500 nm	150°C	No	No	Transparent conductors and sensors

devices require two essential and basic properties. First, the chipless RFID tag needs to be detectable from a range that is compatible with its potential areas of application. Section III-A will discuss the inherent challenges that limit the detectability of such structures, and what solutions are now proposed and implemented in order to tackle them. Finally, RFID structure needs to be able to encode useful information, either for sensing or identification purposes, which can then be extracted from the reading. The different approaches adopted to provide this capability are show in Section III-B.

A. The Rise of Long-Range Chipless RFIDs

As their name suggests, chipless RFID configurations are characterized by their lack of chips (i.e., active components). These should not be mistaken for passive RFIDs, which, contrary to what their name might suggest, are made up of numerous active components. The passive RFID structure and all of its essential components will be described in detail in the next sections. From a conceptual perspective, chipless systems are extremely appealing as possible motes for IoT, SS, and 5G applications. Indeed, the lack of active components removes the need for any power supply (including energy harvesting of any sort), while their minimalist structures allow for these devices to be extremely low cost and generally compatible with large-scale production using AMTs, such as R2R-printing technologies. Many close-range chipless RFID tags have been reported for applications such as wireless barcodes of the IoT and chemical [17], [22], displacement [23], temperature [24], and humidity sensors [25]. Furthermore, almost all of the reported structures are either compatible with printing technologies, or have been manufactured with AMTs, including fully printed chipless chemical sensors, enabled with chemisensitive printed nanomaterial films (such as CNTs, for instance). Nevertheless, their range limitation prevents them from being applicable to most of the potential configurations envisioned for IoT, SS, or even 5G implementations. Recent trends have striven toward extending the range of chipless RFID systems in order to provide low-cost solutions for applications with much more demanding reading range requirements. Very recent implementations of smart structures and reading schemes, which will be presented in the following paragraph, are finally breaking the range limitations.

The fully inkjet-printed structure, shown in Fig. 2, comprises five linear antenna arrays with two isolated ports. The square patch antennas that constitute the fundamental radiating elements of the array structure have two degenerate radiating modes, whose radiated fields are cross polarized; each of the two ports of the linear antenna structure is coupled to only one of the two cross-polarized radiating modes. By connecting ports of each linear array to the cross-polarized port of their symmetrical (with reference to the axis of symmetry of the array) counterpart, using lines of identical electrical lengths (characteristic of the Van Atta configuration), a cross-polarized response with the expected reflection properties can be achieved. This can be observed in the remarkable isotropy of the monostatic radar cross section (RCS) of the electrical large (about 20 λ^2) array structure, shown in Fig. 3.

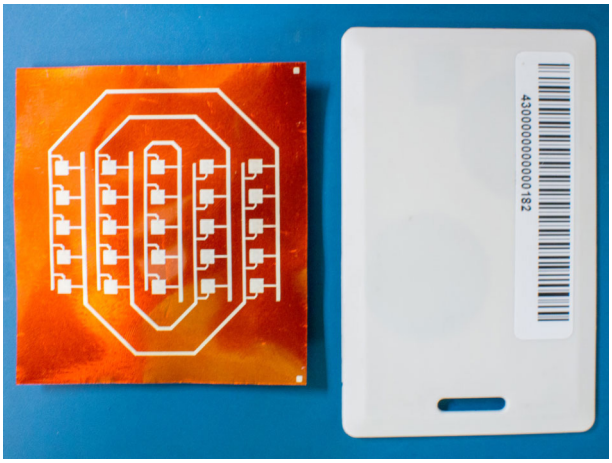

Fig. 2. ***Inkjet-printed flexible Van Atta reflectarray prototype, next to a standard "credit card" size RFID tag package [21].***

Indeed, the RCS only changes by 10 dB over an angular range of 140°. This Van Atta design allows the implementation of all the range-enhancing techniques previously described. Doing so, a benchmarking range of 30.5 m was achieved, in the real environment shown in Fig. 4.

This reported range represented more than a tenfold increase in the range of chipless RFIDs, compared to the state-of-the-art configurations mentioned earlier. Furthermore, the approach has also been demonstrated as being compatible with multitag configurations, where several tags can be differentiated, for the first time, by both their time

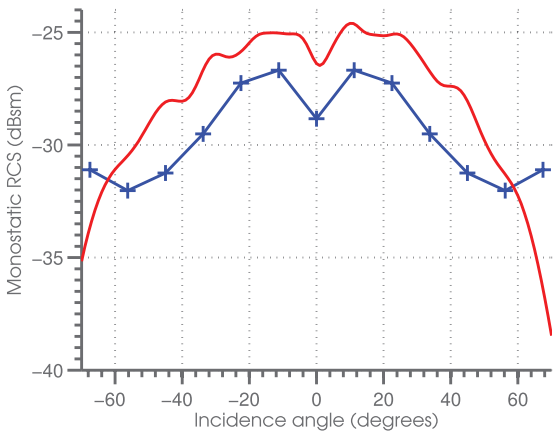

Fig. 3. ***Measured (blue +) and simulated (red solid) monostatic RCS of the Van Atta reflectarray [21].***

Fig. 4. ***Measurement configuration at an interrogation range of 30.5 m [21].***

frequency and time-delay responses, as shown in Fig. 5, therefore providing an additional degree of freedom for tag/sensor identification and sensing-information extraction. Finally, it is worth stressing that this fully inkjet-printed device was implemented in the Ka band (26.5–40 GHz), and could therefore operate at the frequencies envisioned for 5G networks. Coupled with its long range, this opens up the opportunity for the integration of low-cost chipless RFID devices into the structure of upcoming 5G cellular networks.

The field of short-range chipless RFIDs, which are inherently AMT-compatible, has grown tremendously during the last decade, provided a detailed picture of the capabilities of such structures, and demonstrated their applicability for a range of different practical contexts. Furthermore, very recent trends have enabled additively manufactured chipless RFIDs with medium and long ranges of up to few tens of meters. For these reasons, it is reasonable to expect that chipless RFIDs might become the first mass implementation of additively manufactured RF systems and components, in the shape of identification and sensing nodes of the IoT and 5G networks with unprecedented interrogation ranges.

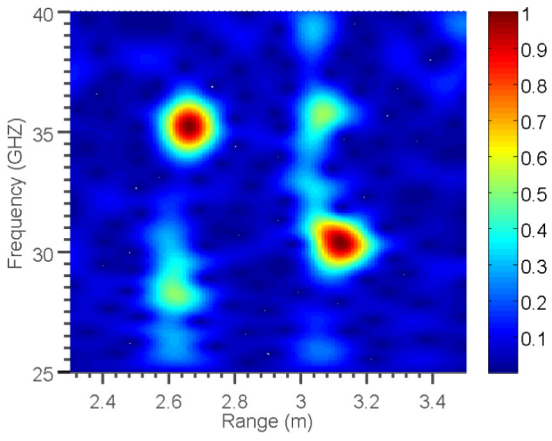

Fig. 5. ***Spectrogram of a measurement in a multitag configuration [21].***

B. High-Density and Reconfigurable Encoding Schemes

After receiving the incoming electromagnetic wave, the RFID tags need to encode the transmitting signal either with amplitude, phase, or frequency, so that the reader can interpret the binary codes that carry the desired information. Just like the ICs in regular RFIDs, chipless RFIDs usually need some certain structures to enforce the encoding. The encoding structure is the key part of chipless RFID operation as it is the foundation of the system working principle and the tag performance. One of the most commonly used methods to encode chipless RFID is by embedding multiple resonators into the tag. The resonant frequencies of these resonators are separated with a sufficient difference, so that each resonance works independently and stands for one bit. In order to represent "1" and "0," the resonant frequency of each resonator features an original value and a shifted value. In fixed-code chipless RFID, this shift is usually performed by shorting the resonator during the fabrication process. These resonant frequency shifts can be detected in several different ways depending on the reader setup. First, the most straightforward method would be identifying the resonance by frequency spectrum sweep, which requires a wide bandwidth operation of the reader in general. Second, the resonator usually shows a bandstop or bandpass feature depending on embedding method so that the signal amplitude at a specific frequency can be used to identify the value of that bit. Third, as the resonance is accompanied by a phase jump, the bit value shows in the phase at a specific frequency as well.

Multiresonator approach methods feature a relatively large data capacity, which can be enlarged by simply increasing the number of resonators embedded. For a limited bandwidth of the RFID system, more bits can be integrated into the tag with a higher Q-factor of the resonator. The size of the tag is another concern in the choosing of a resonator, as a compact size would fit more IoT applications. Up to 35-b chipless RFID realized with spiral resonators was reported [26], [27]. Chipless RFID based on high-Q nested loop resonators presented in [18] shows a 28.5-b data capacity and a very compact size. Slot resonators were also used in chipless RFID tags, so that the size of the tag would not increase with bits [28]. Dual-band resonators were proposed to double the number of bit per resonator [29]. Besides multiresonator approaches, many other structures such as phase delay lines [22], [30] were reported in chipless RFID. Although most prototypes in aforementioned literature are fabricated by traditional subjective print circuit board (PCB)

techniques, most chipless RFIDs have a simple planar geometry, and thus they are compatible with AM techniques such as inkjet printing.

A proof-of-concept prototype of a first-of-its-kind fully inkjet-printed chipless RFID encoding module enabling real-time encoding and fluid sensing [16] is shown in Fig. 6. The key to enable the real-time encoding mechanism is to toggle the binary codes by shifting the resonant frequency of the resonators on the fly. By embedding an inkjet-printed or 3-D-printed microfluidic channel between two adjacent turns of the spiral resonators, the resonant frequencies of the spiral resonators can be shifted by filling or unfilling liquid to the channel. The resonance shifts due to the relative permittivity change from 1 for air to 73 for water [31] inside a gap or a "capacitor," which is widely used in microfluidics-based tunable electronics. A detailed explanation of this mechanism can be found in Section V-E. The code can be toggled between "0" and "1" on the fly for time-varying information while using less than 0.5 μL of water per bit. The encoding capability of this real-time encodable chipless RFID module is shown in Fig. 6(b), where the magnitude values of S21 were measured under all eight codes of configuration for a 3-b code. Here we define "0" and "1" frequency as the resonant frequency of air- and water-filled microfluidic channel, respectively. Given these definitions, the magnitude variance at "0" and "1" frequencies for different code configurations are listed in Table 2, as a summary of the performance of the multiresonator encoding module. Overall, an insertion loss difference of at least 8.4 dB at "0" frequencies was observed, allowing a reader to easily differentiate the bit values. The proposed chipless RFID module maintains a stable performance during bending as shown in Fig. 6(b) and can be bent to radii as low as 12 mm, which shows an excellent flexibility and a great potential in wearable and conformal applications. This encode module also facilitates sensing of various fluids such as identifying different water–glycerol mixtures, since microfluidics sensors are already integrated in the module. This encodable chipless RFID module can be used in various application spaces including healthcare monitoring, food quality sensing, and RFID for time-varying information.

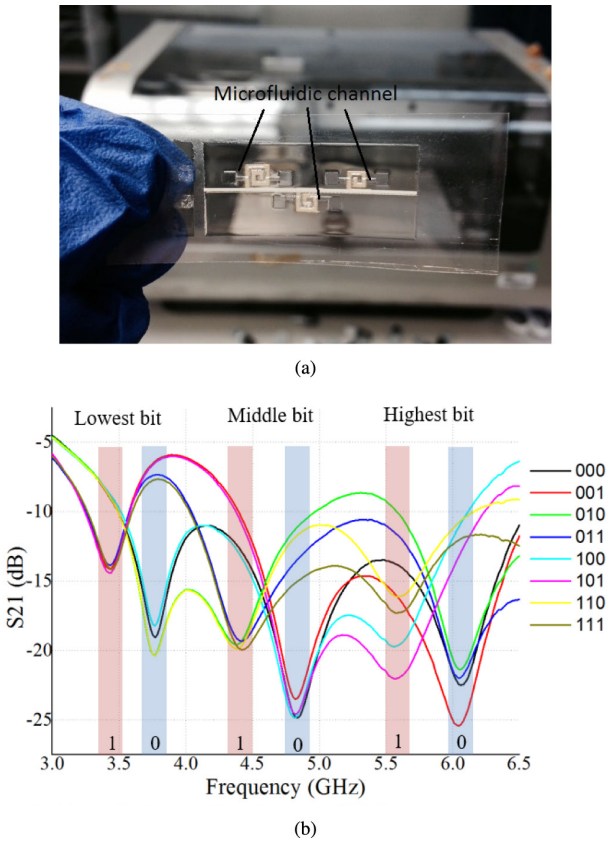

Fig. 6. *(a) Photo of an all-inkjet-printed microfluidics-based encoding module of chipless RFID with an inkjet printer in the background. (b) Simulated and measured insertion loss values of the prototype for code "000" and "111" configurations in flat or bent for a 30-mm radius [16].*

Table 2 "Code" Frequencies for Every Bit and Minimal Attenuation Difference Between '1' and '0' at "Code" Frequencies

Code		'1'	'0'
Lowest bit	Code frequencies	3.44 GHz	3.77 GHz
	Minimal attenuation difference	4.8 dB	10.5 dB
Middle bit	Code frequencies	4.42 GHz	4.84 GHz
	Minimal attenuation difference	6 dB	8.4 dB
Highest bit	Code frequencies	5.57 GHz	6.06 GHz
	Minimal attenuation difference	0 dB	8.5 dB

IV. ENERGY SOURCES FOR SELF-SUSTAINABLE AUTONOMOUS SYSTEMS

Energy is a remarkable aspect for the autonomous operation of any ubiquitous system. Conventional autonomous devices rely heavily on primary batteries, which can power the device only for a certain amount of time. The batteries have to be replaced once the sensor devices use up stored energy in their batteries which increases the cost significantly as the number of sensor devices in the system increases. To avoid this maintenance cost issue and achieve completely self-sustainable low-cost ubiquitous systems for IoT and smart cities, ambient energy-harvesting technology has attracted a lot of interest of research community. Energy-harvesting technologies harness energy from ambient power sources, such as solar, heat, vibration, and electromagnetic waves using transducers, and the harvested energy is stored in energy storage components such as rechargeable batteries and capacitors. The stored ambient energy can maintain the operation of a system by adjusting the duty cycle of the device.

A. Additive Manufacturing for Ambient Energy Transducers

AMT such as inkjet printing, 3-D printing, and screen printing have proven to be a very efficient solution for low-cost RF circuit patterning associated with a high 2-D/3-D resolution and a variety in printable materials. In addition, the wide variety of printable materials allows us to create both the transducers and the energy storage components for ambient harvesting from a variety of energy sources, especially solar and RF energy.

1) *Solar:* Solar power is one of the most commonly used harvesting sources featuring high power levels. It has high power density of 100 mW cm^{-2} during daytime and 100 μW cm^{-2} in indoor environments with a maximum conversion efficiency of more than 45% [32]. The conversion efficiency heavily depends on the materials used for the solar cells. Commonly used materials for low-cost printable solar cells are inorganic perovskite-based inks [33] and organic polymer-based inks [34], with yields of 10.1% and 4.1% of conversion efficiency, respectively. The conversion efficiency of printed solar cells is relatively low compared to silicon-based solar cells, but the solar cells can operate in a hybrid mode in conjunction with other types of energy source to virtually increase the available power per area [35], [36].
2) *Electromagnetic Waves:* Compared to other ambient energy sources, ambient RF energy has a relatively low power density of 2 nW cm^{-2} to 1 μW cm^{-2} in the far field of RF energy source. However, more RF energy can be collected utilizing high-gain antennas. Also, the power density can reach up to 10 mW cm^{-2} in the near field of an RF energy source. The near-field RF energy-harvester circuit depicted in Fig. 7 is fabricated utilizing the inkjet-printing masking technique [37]. The conversion efficiency heavily depends on the available power level, and it can reach to about 90% for input power levels above 100 mW. On the other hand, the efficiency decreases less than 30% when the input power is less than 10 mW, which is a typical value in the far field [37], [38]. Regardless of the low energy density, RF energy harvesting is attractive because of its availability and the small form factor of transducers. In addition to these advantages, RF energy harvesters are well compatible with AMT, especially inkjet printing. For RF energy harvesting, a special type of antenna called "rectenna," or rectification antenna, is commonly used. Typically, the rectenna is composed of an antenna, a matching circuit, and a diode. Specifically, a Schottky diode is commonly used because of its fast switching speed and low threshold voltage. With the development of inkjet-printing technology, passive components in the rectenna, such as capacitors and inductors, circuit traces including antennas, and even substrates can be created utilizing printing technology [2], [39]–[41]. Recently, Sani *et al.* have reported that the diodes for RF rectification can be fabricated with a combination of printing technologies [42].

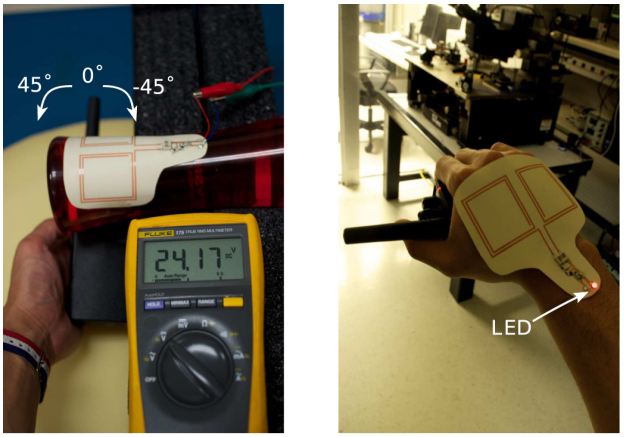

Fig. 7. *(a) Open voltage measurement of near-field harvester with an on-bottle setup. (b) Operation verification of the near-field harvester on the hand.*

B. Additive Manufacturing for Energy Storage Devices in Autonomous RF Systems

Once each transducer converts the ambient energy into electric energy, it is stored in energy storage devices, such as a battery and a capacitor. They can be classified into three types depending on the operation principle: dielectric capacitors, electrochemical capacitors (electric double layer capacitors and pseudocapacitors), and batteries. Each device has different area-specific capacitance and discharge speed, which determines the maximum power.

1) *Dielectric Capacitors:* Dielectric capacitors are well know as parallel plate capacitors, which are composed of two metal plates separated by dielectric materials. In the presence of an electric field, charges are directly stored on the plates as free electrons. The amount of charge is determined by the size (A) and separation distance (d) of the electrodes and the dielectric constant of the material between two electrodes. Since this type of capacitors does not require any chemical reaction in the charge and discharge process, they have the highest power density among the three energy storage devices, although the area-specific capacitance ($\epsilon_0\epsilon_r/d$) would be less than 0.02 Fm^{-2} even with very high dielectric constant materials ($\epsilon_r = 2000$) for $d = 1\mu$m. Cook *et al.* have reported dielectric capacitors fabricated only using inkjet-printing technology which can support the operation up to RF range [40].

2) *Electrochemical Capacitor:* Electrochemical capacitors store charges on the surface/subsurface rather than in a bulk material as in batteries. Depending on charge storage mechanism, electrochemical capacitors are classified into electric double-layer capacitors (EDLCs) and psuedocapacitors. EDLCs store charges due to accumulation of ions on the surface without involving conventional dielectric materials. EDLCs do not have any chemical reaction, so the power density is as high as dielectric capacitors, and the area-specific capacitance would be 0.1 F m^{-2} with $\epsilon_r = 10$ and $d = 1$ nm because of the extremely small separation distance. In contrast, pseudocapacitors, which are also known as supercapacitors, involve fast and reversible redox reaction on the surface/subsurface of the electrodes. The pseudocapacitors have higher energy density than EDLCs, which can go up to 1500 F g^{-1} [43]. Chen *et al.* have reported supercapacitors with an energy density of 138 F g^{-1}, fabricated using an inkjet printer [44].
3) *Battery:* Batteries charge and discharge electricity through chemical reactions. Rechargeable (secondary) batteries are usually needed for energy-harvesting applications. Since they involve chemical reactions, it requires relatively long charge/discharge time in the order of a few minutes to a few hours. A variety of materials such as nickel cadmium and lithium ion can be used as electrolytes, but for printed batteries, a zinc polymer is typically used because of its low toxicity, thin form factor, and low cost [45]. Their energy density can be 100 W h L^{-1} to 300 W h L^{-1}.

V. ADDITIVELY MANUFACTURED RF PASSIVE COMPONENTS AND PACKAGING STRUCTURES

With the emergence of mm-wave wireless technology for 5G and automotive radar applications, focus is being placed on both the miniaturization and highly efficient integration of interconnects, sensors, and passive components for mm-wave systems. All of these considerations are also key for future printed IoT and 5G motes. In order to realize these systems, SoP design schemes are of interest in fully integrated 3-D RF topologies for the reduction of loss between mm-wave components in a fully integrated wireless topology. Current mm-wave systems use common industry-standard interconnection solutions, such as wire bonding and flip-chip techniques. Though well established in the field of low-cost microelectronic packaging, wire bonding has the potential to yield high parasitic inductance requiring additional passive component compensation in the high mm-wave regime [46]. Flip-chip techniques reduce interconnection length and parasitics yet are often victim to high sensitivity to coefficient of thermal expansion (CTE) mismatch and detuning from the close proximity of active circuitry to peripheral packaging interconnects [47]. Moreover, such techniques are incompatible with fully printed systems fabrication. Similarly, realization of a low-cost, miniaturized SoP design would require the efficient design and integration of different RF components using AMTs. This section highlights some of the ground-breaking work in design of interconnects, passive components, flexible components, and IC encapsulation methods for SoP solutions using AMTs. These techniques, even though often applied as a complement to traditional packaging approaches, are now providing an essential set of tools for the fabrication of future fully printed IoT and 5G motes.

A. Inkjet-Printed Interconnects

Interconnects create an electrical pathway between one or more layers of a multilayer electrical and the RF structure and play a vital role in the fabrication of low-cost, compact, and highly dense multilayer IoT, SS, and 5G nodes. They can be divided into three categories: through-hole vias, buried vias, and blind vias. Through-hole vias connect all the layers and are exposed at both the top and bottom; buried vias are not exposed on either side and connect intermediate layers; while blind vias connect some layers that are exposed on only one side. However, vias can introduce parasitic inductance and capacitance, thereby affecting the overall performance of the device. Moreover, the design is further complicated for flexible structures where the vias can crack under bending and create unwanted local reflections and standing waves. Therefore, efficient interconnect/via design is essential for high-performance RF circuits and components. In this section, we present some state-of-the-art techniques to realize additively manufactured interconnects. Typically, vias are formed by physically etching the substrate and filling the holes using inkjet printing or conductive epoxy to create an electrical short between layers. However, this approach is problematic as it complicates the alignment process and the via dimensions would depend on the etching mechanism. While drilling is a simpler and much cheaper option as compared to liftoff or other subtractive processes, it is inefficient and further complicates both alignment and printing operations. On the other hand, via realization is relatively simple for both thick and thin substrates using AMTs such as inkjet printing because it directly prints on the substrate to create vias and/or metallize via sidewalls.

Previously, various techniques have been used to realize microvias. These include etching the substrate with a laser [49], using inkjet printing to dispense droplets of ethanol ink to create a crater-like structure [50], or printing the via itself in a layer-by-layer fashion [51]. Later, the via sidewalls are inkjet printed with conductive ink for metallization and create an electrical short between the layers. In [52], a stepped via approach was used to realize vias on relatively thick substrates with a diameter of 2 mm and conductivity of $7.4 \pm 2\Omega$.

The first-of-its-kind fully inkjet-printed multilayer "drill-less" vias and "through-substrate" conductive traces are presented in [48]. These use the porosity of the normal (110-μm-thick) cellulose paper to absorb the conductive ink into the substrate and create an electrical short within the fabric of the paper. It was shown in [48] that the SNP ink goes through almost half the thickness of the cellulose paper when ten or more layers of SNP ink were printed on one side of the paper. Hence, "drill-less" vias were realized by printing ten layers of conductive SNP ink on both sides of the paper and curing it for 2 h at 150 °C. The cross-sectional view and surface profile of cellulose paper for different numbers of SNP layers is shown in Fig. 8, while the direct current (dc) resistance of "drill-less" vias for different numbers of layers is given in Fig. 9. In order to verify the performance of the inkjet-printed vias under bending, a fully inkjet-printed substrate integrated waveguide (SIW) was fabricated on cellulose paper, as shown in Fig. 10, and bent at different radii of curvature. It appeared that the performance of the SIW was not significantly affected under bending, as shown in Fig. 11. This was attributed to the fiber-like bulk structure of the printed silver within the paper, which tends to have the capability to accommodate for a large amount of stress without breaking.

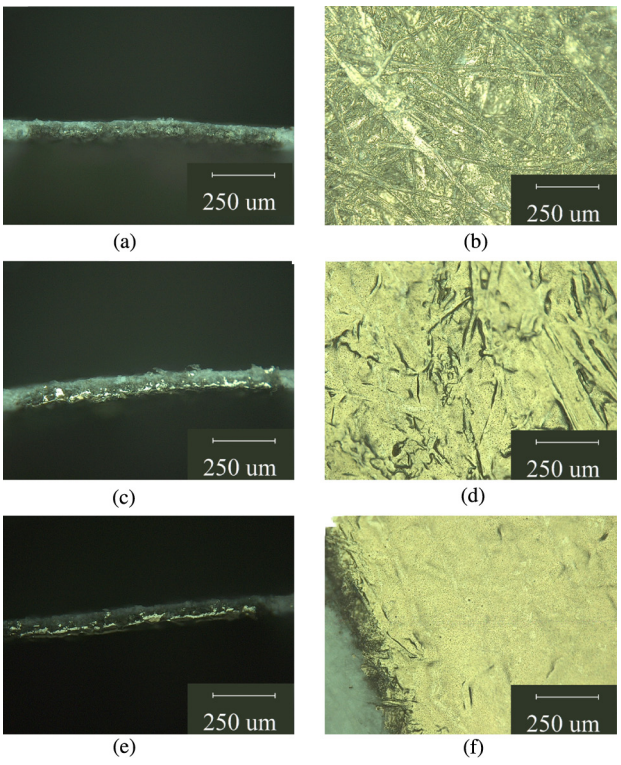

Fig. 8. ***Cross-sectional view and surface profile of 1-mm-wide inkjet-printed lines with SNP ink for different number of layers [48]. (a) 1 layer cross sectional view. (b) 1 layer surface profile. (c) 5 layers cross sectional view. (d) 5 layers surface profile. (e) 10 layers cross sectional view. (f) 10 layers surface profile.***

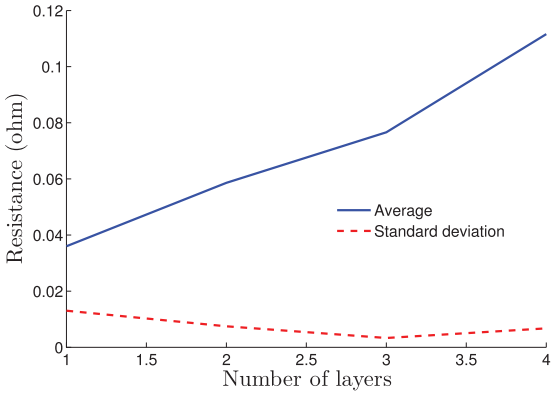

Fig. 9. ***Average value and standard deviation of dc resistance of multilayer vias on cellulose paper.***

Moreover, exploiting the robust nature of inkjet-printing technology for electronic fabrication, mm-wave interconnects can be designed and implemented through additive means to realize flexible, efficient, and highly integrated wireless systems. Unlike traditional wire bond and flip-chip interconnect technologies, inkjet printing is able to directly fabricate canonical transmission line structures within a wireless package to interface IC dies, passives, sensors, and other desired peripherals [53]. Fig. 12 graphically outlines the typical stackup of an inkjet-printed 3-D mm-wave interconnect. First, a die is attached to a packaging substrate with a printed adhesive ink material. Once the die is adhered, dielectric ramps are inkjet printed with a thick dielectric ink in order to bridge the top of the IC die to the packaging substrate below. Finally, conductive ink is printed to pattern low-loss coplanar waveguide (CPW) transmission lines, to route the mm-wave signals from the die to any desired peripherals in/on the package.

The components of this fully printed packaging solution are realized with both dielectric SU-8 epoxy-based and SNP-based inks to pattern dielectric ramps and attach structures along with metallic transmission lines, respectively. Images and measurements of these printed 3-D interconnects are

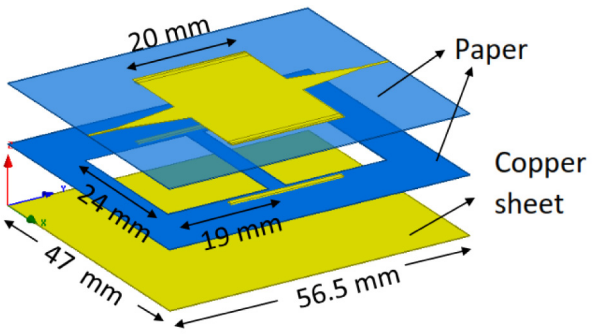

Fig. 10. ***Exploded view of fully inkjet-printed SIW [48].***

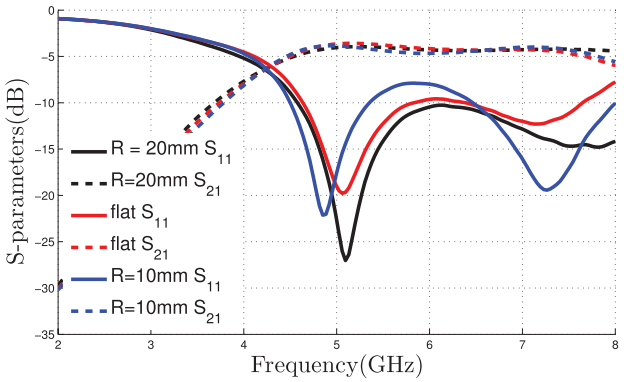

Fig. 11. ***Variation in measured S-parameters of the inkjet-printed SIW prototype with solid sidewalls for different radii of curvature [48].***

shown in Fig. 13. Measurements of the printed samples yield an insertion loss at 40 GHz of 0.6–0.8 dB/mm with a matching below −10 dB across the measured band. Inductance is measured to be 0.4–0.5 nH/mm, yielding half of what is typically achieved through standard wire bond techniques [54]. This demonstration of inkjet-printed mm-wave 3-D interconnects highlights the capabilities of this rapid prototyping technology for wireless SoP solutions in the emerging field of highly integrated mm-wave systems.

B. Inkjet-Printed Passive Components

Passive components are integral pieces to any RF system, being extensively utilized for matching networks, filters, signal tuning, and noise reduction. In order to avoid high-profile, rigid lumped components and eventually enable the advent of fully printed systems, inkjet printing is used to realize capacitive and inductive RF structures to enable low-profile and flexible systems in an efficient additive fashion. The fundamental metal–insulator–metal (MIM) capacitor is a well-established RF passive component in inkjet-printing technology realized by the multilayer printing of silver nanoparticle and thin polymer dielectric inks, yielding high per-unit-area capacitance and a self-resonant frequency (SRF) above 1 GHz [8]. Multiturn spiral inductors are realized through the integration of silver nanoparticle and thick dielectric inks for spiral patterning and additive via patterning, respectively, yielding high per-unit-area inductance, quality factors (Q) exceeding 20, and an SRF above 1 GHz [8].

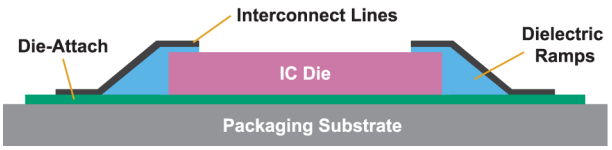

Fig. 12. ***Graphical stackup of inkjet-printed 3-D interconnects for mm-wave systems [53].***

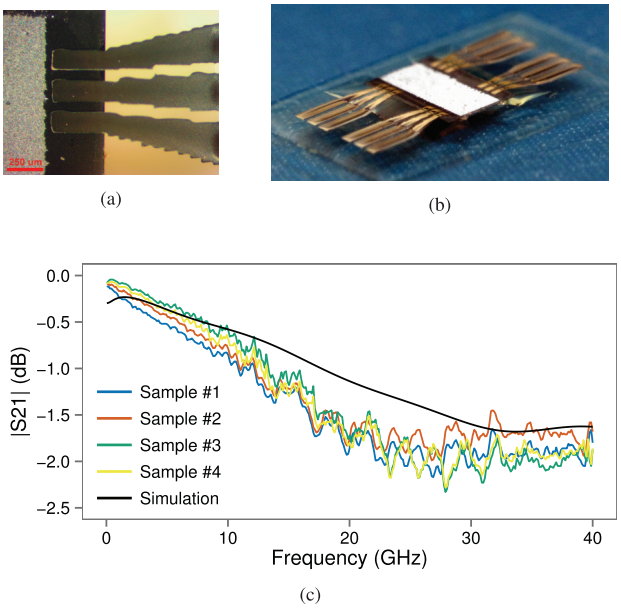

Fig. 13. ***(a)–(b) Micrographs of inkjet-printed 3-D mm-wave interconnects. (c) Insertion loss of fabricated CPW transmission lines from die to packaging substrate [53].***

Taking advantage of the multilayer nature of inkjet-printing fabrication, complex passive structures typically requiring multiple laminate substrates are realized using a single host substrate with conductive and insulating inks. An example of these methods is highlighted in the demonstration of a fully inkjet-printed 3-D transformer balun [55]. The transformer design, shown in Fig. 14(a), consists of a center-tapped three-turn primary coil in parallel with a two-turn secondary coil, a topology typically used to increase power transfer efficiency in practical consumer applications. As highlighted in Fig. 14(b), the transformer design consists of five distinct layers, all patterned on a flexible LCP substrate. These layers are realized with silver nanoparticle-based ink for the conductive traces and SU-8 epoxy-based ink to pattern the thick dielectric bridges for multilayer signal routing. The fully inkjet-printed five-layer balun transformer is shown in Fig. 14(c), demonstrating a fully printed highly complex RF passive component fabricated on a flexible RF substrate for rollable, conformable, and fully additively manufactured, RF systems.

In addition to the capability of multilayer fabrication, another enabling aspect of inkjet-printing process for passive components fabrication is the freedom to print RF structures on virtually any host substrate. On-silicon passives, specifically capacitors, are useful in decoupling circuits for the suppression of noise in mixed-signal circuit technology. Utilizing both thin and thick dielectric inks with metallic inks, fully inkjet-printed multilayer MIM capacitor structures are fabricated directly onto a host silicon substrate [56]. Fig. 15 shows the 3-D material stackup, printed sample, and measurement setup environment for a fully inkjet-printed on-silicon MIM RF capacitor. First, a

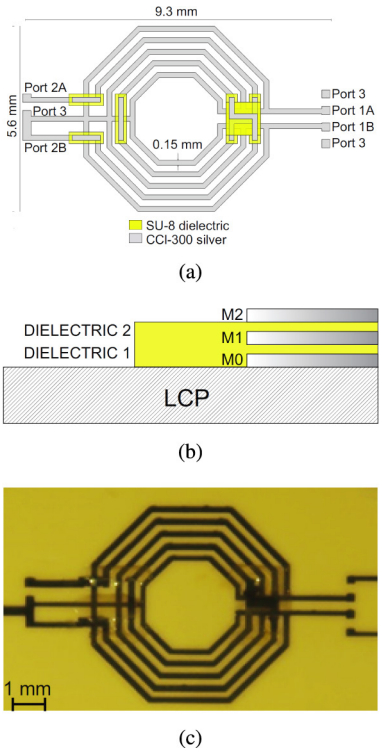

Fig. 14. ***Fully inkjet-printed multilayer balun transformer: (a) model; (b) 3-D stackup; and (c) sample [55].***

thick (20 μm) passivation film is patterned using an SU-8 epoxy-based ink in order to provide isolation from the lossy silicon below the desired passive. Next, the MIM topology is fabricated using a silver-nanoparticle-based ink for the circular plate electrodes and a poly (4-vinylphenol) (PVPh)-based ink for the thin (1.6–1.8 μm) insulating dielectric. This fully printed on-silicon passive yields a per-unit-area capacitance of 33 pF mm^{-2}, a maximum Q of 25, and an SRF at 1.2 GHz, measurements that exceed current state-of-the-art inkjet-printed passives even while operating on a lossy silicon host substrate. The additive and postprocess aspects of these passive components allow for the miniaturization and increased system-level integration of wireless RF and microwave devices from a SoP design solution standpoint, as well as the prospect of fully additively manufactured mm-wave systems and components.

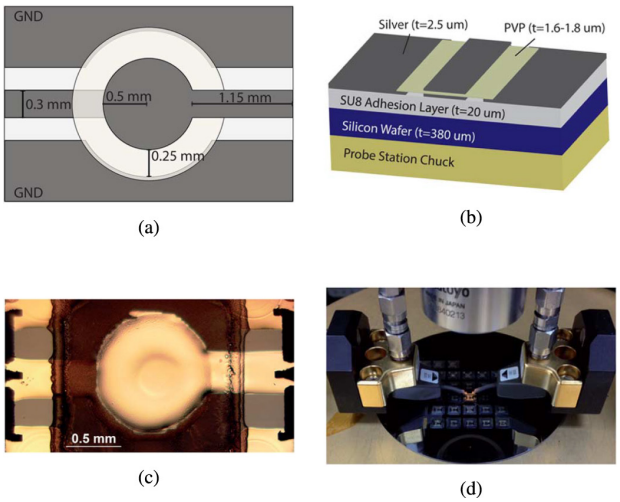

Fig. 15. ***Fully inkjet-printed on-silicon MIM capacitor: (a) model; (b) 3-D stackup; (c) sample; and (d) measurement setup [56].***

C. Stretchable Electronics

Whereas most AM designs may require minor modifications to conform to complex topologies, stretchable electronics allow for the fabrication of RF designs, which can more easily conform to unique and dynamic surfaces such as high curvature profiles on rigid materials or fabrics, ideal for wearable RF devices, smart skins, and IoT. A consequence of stretching is the deformation of size controlled devices, with microstrip lines, antennas, and dielectrics dynamically changing in widths and thickness. These new constraints lead to uniquely challenging design approaches, which may accommodate for these variations. A common dielectric material for RF stretchable structures is silicone, due to its compatibility with biological bodies.

There are multiple ways to approach stretchable RF electronics. A common methodology is to employ traditional metal films that are formed in spring-like structures that deform in order to expand as the base substrate is stretched. This allows for controlled conductor widths, as the spring-like pattern does not stretch but rather flexes, which may lead to more predictable RF designs, but may cause the structure to lift or tilt out-of-plane in relation to the substrate [57]. Alternatively, liquid–metal alloys, often partially consisting of gallium, can be used in conjunction with inkjet-/3D-printed microfluidic channels to enable stretchable designs. Recent advancements have allowed the photolithography-compatible fabrication of stretchable circuits which utilize biphasic solid–liquid thin metal films that enable the fabrication of layers that are as thin as 60 nm [58]. Stretchable inkjet-/3D-printable electrically conductive adhesives (ECAs), often based on a epoxy polymer matrices with silver fillers, also offer an appealing option. A remarkably high-performance silicone-based ECA, utilizing silver flakes and a silicone filler, has been reported in [59]. Its remarkable properties are the product of a weaker curing shrinkage compared to epoxy-based ECAs, which allows this silver-flake-based ink to crosslink with the silicone substrate while avoiding delamination during the postcuring process. The material can be direct printed, enabling compatibility with FDM/direct-write 3-D printers.

While traditional consumer level FDM printing utilizes the process of extruding pastes through commercial syringe needles, with diameters of ~150–200 μm (corresponding to approximately 27–30 gauge needles), flow control can become

Fig. 16. ***Three-dimensional-printed RF hand gesture sensor with silo-ECA on silicone [60].***

an issue due to the internal pressures and lack of valves at the needle tip. High-resolution 3-D FDM and direct printing of metal pastes can be achieved utilizing an nScrypt printer, which contains a unique dispensing system capable of printing pastes from 1 to 1 000 000 centipoise (cP) with a minimum feature size of 12.5 μm. These feature sizes and repeatable fabrication processes were utilized to fabricate a 3-D-printed wireless hand gesture sensor. The hand gesture sensor uses a silicone dielectric, with the nScrypt used to direct print the silo-ECA onto the substrate. The design consists of four spiral resonators operating in the 2.2–3-GHz range, with the resonant frequencies of the resonators separated by 200 MHz from one another, as shown in Fig. 16. With the resonators laid out such that the spacing between them is similar to the spaces between fingers, the resonators fluctuate in operational frequency based off the stretching of the resonators and the change in the coupling gap, leading to the ability to sense strain in a multibit chipless RFID manner.

D. "Shape Changing"/Morphing (4-D-Printed) RF Structures

One of the key drawbacks of conventional RF structures is that they are unable to reconfigure their mechanical, RF, and electrical properties with respect to changes in their ambient environment. That is why most of the RF passive components such as antennas, filters, etc., can only operate within the designed frequency bandwidth for a particular application. However, the number of RF components as well as the overall size of the system can be drastically reduced using reconfigurable and tunable RF structures. Traditionally, this can be achieved by using varactors [61], [62] (FSS), diodes or using special types of substrates such as liquid crystals [63]–[65], or ferrites [66] which can produce a 15%–20% frequency shift by changing their properties using external excitation.

Alternatively, the RF characteristics can be varied by using "shape-changing" 4-D-printed RF structures that change/morph their behavior on demand when actuated. A recent example of such structures is presented in [68] which uses an origami inspired reconfigurable antenna that changes its resonance frequency by mechanically varying its height. The advantage of such antennas is that they are extremely light weight, compact, and can be tuned to a relatively wider range of operational frequency as compared to other methods mentioned earlier. That is why they have found many applications in space [69], biomedical [70], and deployable mechanical structures [71].

However, the implementation of flexible conductive traces is the key to additively realizing such "shape-shifting" 4-D-printed structures. This can be achieved by using either flexible conductors, custom-made substrates such as cellulose nanofiber paper [72], or using special structures along the bends, as mentioned earlier in this section. A novel design to realize a fully inkjet-printed tunable frequency selective surface (FSS) using a traditional Miura structure is shown in Fig 17(a). The geometry of a typical Miura unit cell is shown in Fig 17 and is completely defined by two angles (θ and β) and two lengths (l_1, l_2). A simple dipole-based FSS is employed in this effort for proof-of-concept demonstration using inkjet-printing technology. The structure was realized by first printing Miura folding pattern on 110-μm-thick cellulose paper using perforations. The dipole patterns were then printed on the mountain fold of the Miura as shown in Fig. 17 using the technique outlined in [48]. Finally, the mountains and valleys were formed by folding the paper along the perforations. The simulated and measured results for variation in operational frequency with respect to changes in angle θ are shown in Fig. 18. A detailed

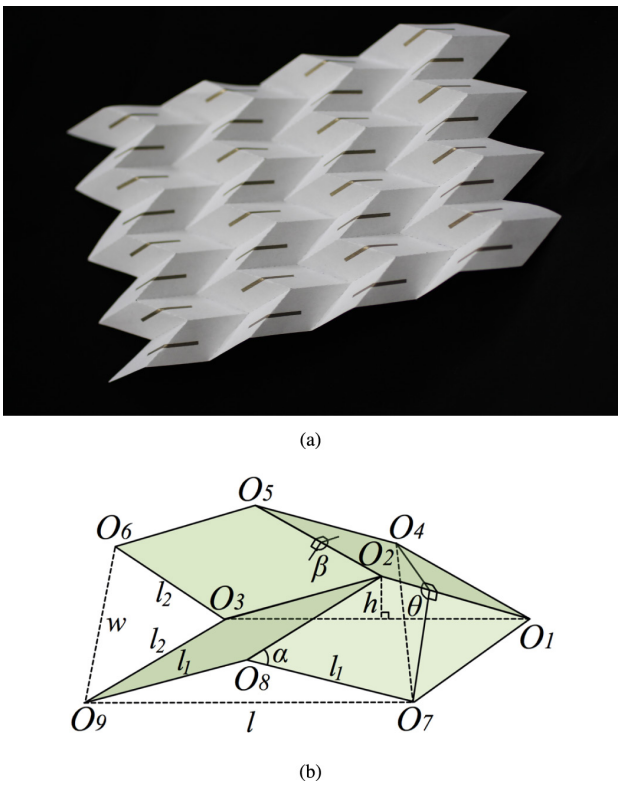

Fig. 17. ***(a) Photo of a fully inkjet-printed shape-changing FSS based on the Miura origami structure on the flexible substrate. (b) Miura unit cell [67].***

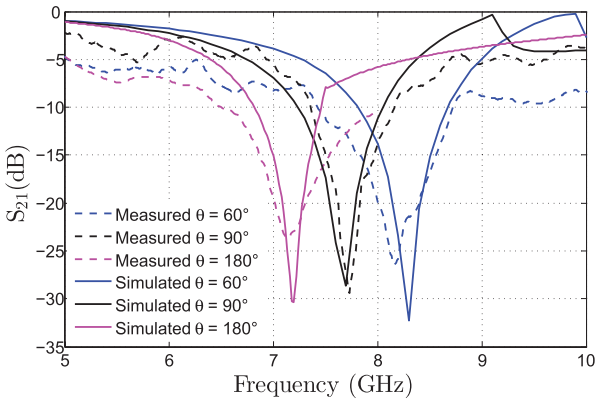

Fig. 18. ***Simulated and measured results for variation in operational frequency of the inkjet-printed Miura FSS with change in angle θ.***

analysis of Miura kinematics and its response to different design parameters will be outlined in future work.

E. Additively Manufactured RF Sensing Elements for IoT and 5G Motes

The potential to provide low-cost RF motes for ubiquitous sensing in the IoT, remains one of the main (if not the most prominent) appeals of additively manufactured RFID systems. In order for this vision to become reality, most or all of the components of such systems would need to be additively manufactured, therefore providing unprecedented cost efficiency. One of these essential components is, of course, the sensing element. In this section, recent advances and trends in the development of AM-compatible sensing components will be presented. The next sections will cover, consecutively and respectively, the fields of chemical-based sensors and that of permittivity-based microfluidic sensors.

1) *Chemical Sensors:* Current film-based electrical gas sensing elements usually rely on two distinct structures. On the one hand, amperometric and potentiometric elements rely, respectively, on the current produced by an ongoing chemical reaction [81] or the equilibrium electrochemical potential of a cell [82] for sensing. On the other hand, resistometric/conductometric/impedometric (RCI) sensors use the changes in impedance of a sensing film in order to signal the presence of an analyte.

From a fabrication and materials standpoint, these categories have a small but significant difference: amperometric and potentiometric sensors require the use of an ionic bridge between the electrodes, either in the form of a gel or of a liquid solution. If the chemical sensor is placed into a liquid phase environment, the liquid can act as that ionic bridge. For this reason, these types of sensors are extremely well suited to liquid phase sensing, and have, as a consequence been demonstrated in numerous reports (targeting a range of analytes that is too broad to list in this section) for this purpose. In this context, their structure is extremely compatible for fabrication with AMTs, as coplanar printed electrodes (which might be subsequently surface functionalized) comprise the entirety of the structure. In gas media, however, the structure requires a carefully packaged electrolyte (usually a gel) which adds a level of complexity to the fabrication process. As a consequence, examples of such printed structures are exceedingly rare. Nevertheless, recent progress in the AM of thin electrolytic materials [83], [84], motivated by their advantages as gate dielectric material for printed transistors, are opening new opportunities within this field. Such an implementation has even been reported as used as a component of a printed far field wireless sensing system [85].

Due to the lack of requirement for an ionic bridge, and enabled by the rise of nanotechnologies and conductive polymers, RCI gas sensors have been the subject of a very prolific area of scientific research. Most efforts rely on metallic electrodes which are only connected by a film of active material. While the traditional implementations of such sensors, developed at Bell Labs in the 1950s [86], relied on semiconductor crystals (heated at temperatures in excess of 1000 °C) as their active material, current implementations have focused on films of nanostructured materials [such as a thin mats of carbon nanotubes (CNTs) or PEDOT:PSS] because of their extremely high surface area. The focus on such materials, which can easily be extruded or printed through thin nozzles, has given birth to a wide range of high-performance gas sensors whose structures are extremely well suited for AM.

For reference, Table 3 presents a shortlist of such state-of-the-art sensors, their targeted analyte, sensing performance, and active material. The advantages of the generation of RCI described in the previous paragraph has led to their implementation into fully inkjet-/3D-printed wireless structures, such as chipless RFIDs and passive RFID configurations, for the detection of analytes such as NH_3 [17], [22], [87], [88],

Table 3 List of Notable Resistometric Gas Sensors, and Their Sensing Materials and Performance

Ref.	Analyte	Lowest detected concentration and associated sensitivity	Sensing materials
[73]	H_2	30% at 3 ppm	SiNW/Pd
[74]	CO_2	10% at 10 ppm	Graphene
[75]	NH_3	60% at 10 ppb	PANI-PSS NP
[76]	NO_2	5% at 100 ppt	CNT-PEI
[77]	CO	2.2% at 10 ppm	MWCNT
[78]	CH_4	1% at 6 ppm	SWCNT-Pd
[79]	DMMP	150% at 1 ppb	SWCNT
[80]	Nitrotoluene	1.5% at 54 ppm	SWCNT

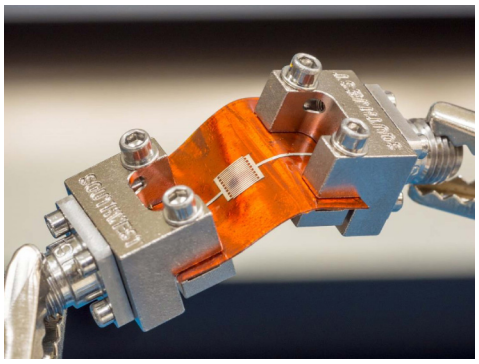

Fig. 19. *Flexible, fully inkjet-printed SWCNT-based IDE structure [90].*

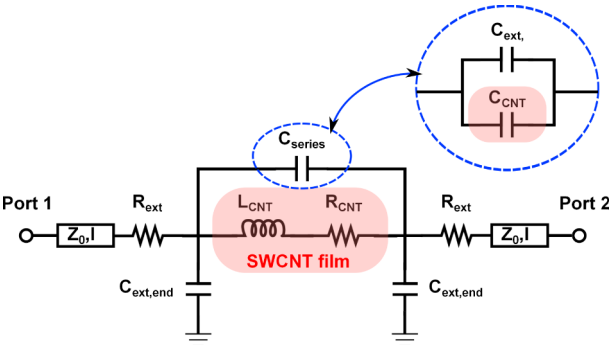

Fig. 20. *Equivalent circuit of the fully inkjet-printed sensing IDE structure [90].*

or humidity [89]. Nevertheless, such implementations have mostly relied on holistic approaches to the system, without describing (and, therefore, not relying upon) a detailed RF characterization of the printed sensing component. Next paragraph presents a rare example of such a fully printed chemical (breath) sensor whose RF properties were carefully characterized.

In this effort [90], the authors characterized the properties of a fully inkjet-printed CNT-based breath sensor (shown in Fig. 19), at frequencies ranging from 500 MHz to 2 GHz. A lumped element model of the sensing element, based on electrical considerations of the interdigitated electrodes (IDEs) and assumptions made on the properties of the CNT film, was assumed and is shown in Fig. 20. The measurements before and after a sensing event were fitted, using an optimization on the component values, following a least square metric upon the complex transmission and reflection coefficients. The fitted component values of the model (shown in Table 4) were extracted. In order to provide a higher accuracy of the fitting, an additional component (a parallel capacitor) was added to the preassumed RF model of the inkjet-printed CNT film (shown in Fig. 20). The final results of this fitting process provided a very accurate model, displaying less than –30-dB relative maximum complex distance between measured and fitted S-parameters over the entire frequency band. Furthermore, as can be seen in Table 4, the model only showed, upon sensing, variations of the components associated with the reactive CNT film (intrinsic), and not those associated with the electrode structure (extrinsic), and therefore confirmed the adequacy of the assumed lumped element model.

Additively manufactured RF chemical sensors feature a number of properties which are opening a promising future toward their integration as sensing elements for fully printed motes of the IoT and 5G networks. First, their ease of fabrication with AMTs, coupled with the forecasted decrease in the cost of nanomaterials, is a strong positive sign toward their ability to provide low-cost solutions for the devices and modules envisioned in this paper. Furthermore, their high sensitivity toward numerous analytes, ranging from byproducts of food rotting processes (such as NH_3), to chemical warfare agents [91], is also making a strong case for their future integration into high-performance wireless chemical sensing systems. Finally, as shown previously, such sensors have been demonstrated and characterized in RF configurations, therefore demonstrating their potential for optimal RF integration on virtually any substrate.

2) *Microfluidic Sensors:* Microfludics refer to the techniques and structures that are used to control extremely small quantities of liquids, and is widely used in manufacturing control, biomedical sensing, chemical assay, and IoT applications [92], [93]. Being "micro" (i.e., compact in size) in nature, microfluidic structures can be easily embedded into various devices, including electronic/RF devices. Therefore, microfluidics can naturally provide application in both tunable RF electronics [16], [94]–[98] and wearable sensors [93], [99]–[102].

One major application of microfluidic RF sensors is real-time biomedical monitoring. With the growing and ageing of the global population, remote biomonitoring, powered by wireless sensors and IoT system, is overtaking the traditional hospital-focused model [103], as a way to enable real-time patient-progress tracking without disrupting the patient's regular life. The real-time monitoring of bodily fluids, such

Table 4 Optimized Component Values of the Equivalent Circuit in Initial and Detection States, and Their Relative Variations [90]

Case	Components					
	R_{CNT} (Ω)	L_{CNT} (nH)	C_{series} (pF)	$C_{ext,end}$ (pF)	R_{ext} (Ω)	l (mm)
Initial	25.1	1.29	3.86	1.31	7.36	3.14
Detection	40	1.81	2.60	1.32	7.21	3.12
Relative change (%)	59	41	-33	0.8	-2	-0.3

Table 5 Permittivity of Different Fluids/Air at Around 3 GHz and 300 K [31], [106], [107]

Name	Permittivity	
	Real part	Imaginary Part
Air	1	0
Hexanol	3	1
Glycerol	4	0.4
Ethanol	6	7
Water	73	8

as tears, sweat, urine, and blood, performed by patients themselves or by medical centers, could be an excellent way to track patient health status and alert patients in time to prevent any life-threatening situations. In this background, micro-total-analysis (μTAS) or lab-on-a-chip (LOC) [104] as well as microfluidics are naturally becoming important technical tools to realize the desirable RF wearable sensors [105].

As common liquids in natural environments feature a wide permittivity distribution at microwave frequencies [31], [107], [108], as shown in Table 5, fully printable RF structures that are sensitive to permittivity variance, such as a gap with strong E-field, can work effectively in sensing the permittivity inside the channel. The permittivity values contain information including but not limited to mixing ratios, concentration, pureness, and temperature. Therefore, if a device can detect small changes in the permittivity values of a liquid solution, a significant amount of information can be deduced from it. One effective and straightforward way to read this permittivity information is to overlay a microfluidic channel on top of a gap so that the capacitance of the gap is modulated by the permittivity of the liquid inside the channel [16], [95], [100], [101]. Embedding the microfluidics channel into the substrate to change its effective permittivity and thus modify the electrical length [96] or the characteristic impedance [102] is another viable approach. Changes such as capacitance variations can be utilized to tune the performance of the microwave structure in the form of detectable shifted resonant frequencies. An overall block diagram of the sensing mechanism is shown in Fig. 21. Besides permittivity, conductivity or resistance of the liquid is another major parameter typically used in fluid sensing, especially for applications such as salts solution concentration monitoring.

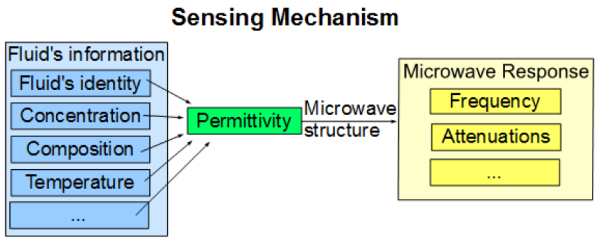

Fig. 21. ***Sensing mechanism of microfluidic permittivity-based sensors.***

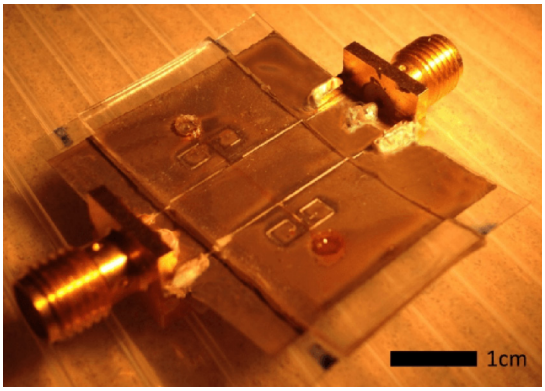

Fig. 22. ***Additively manufactured "peel-and-replace" microfluidic sensor prototype [100].***

High-Q microwave resonators are largely used in permittivity-based sensors because their bandstop feature is easy to detect with a radio system or portable vector network analyzer (VNA). One example of the aforementioned microfluidic sensor can be found in Fig. 22, which is an additively manufactured microfluidics-based flexible RF sensor, potentially enabling "real-world" wearable "smart skin" applications.

A dual-spiral-shaped slot resonator is embedded into the two ground planes of a coplanar waveguide (CPW) with a microfluidic channel embedded in one slot of the resonator. The sensor utilizes two separate parts: a microwave structure and a microfluidic channel. With a reversible sealing, the sensor can be simply "peeled" and "replaced," which facilitates a very wide sensing range by using a microfluidic part consisting of a small-size channel, and a better sensitivity while dealing with low permittivity fluids by replacing it with a larger size channel. With inkjet printing allowing the use of flexible substrates, the sensor features an excellent flexibility, to facilitate wearing scenario such as shown in the inserted photo in Fig. 23(a). Using this proof-of-concept microfluidic channel, seven different fluids were used to measure the sensitivity of the prototype, as shown in Fig. 23(a) and (b), and an overall sensitivity of 24%/ $\log(\epsilon_r)$ was observed, which is superior compared to other microfluidics sensors. In Fig. 23(b), the insertion loss measurement of different mixture ratio can be clearly differentiated. This sensor is fabricated additively and cost-effectively by combining inkjet-printing silver and dielectrics patterning using soft lithography.

While the first microfluidic prototype was fabricated by photolithography, a conventional planar manufacturing technique that is generally expensive and environmentally unfriendly, Whitesides [110]–[112] reported the successful lower cost fabrication of flexible microfluidics using the soft-lithography technique. Recent years have also witnessed an increasing number of AM approaches being proposed to address these issues. Inkjet printing has been

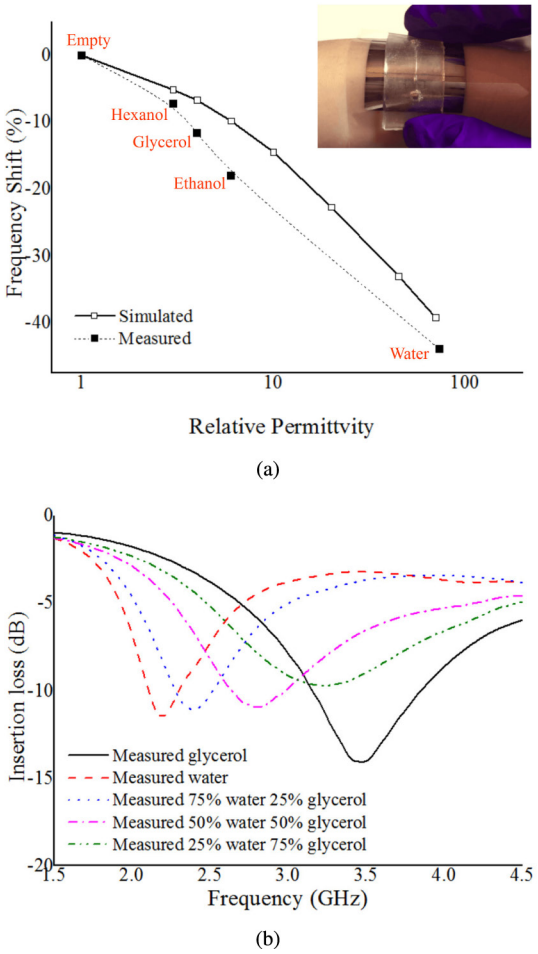

Fig. 23. *(a) Measured and simulated values of the resonant frequency shift for different relative permittivity fluids in the channel of the additively manufactured RF sensor prototype in Fig. 27, demonstrating a logarithmic linearity of sensitivity with an inserted photo of wearing the sensor on the wrist. (b) Measured S21 magnitude values for glycerol–water mixtures with different mixing ratios in the channel, verifying the capability to clearly distinguish mixtures with different mix ratios [100].*

recently introduced in the microfluidics fabrication process [93], [113], and the first fully inkjet-printed microfluidics sensor was presented [102], [109], demonstrating a very attractive minimal channel cross-section area of 38 μm^2 and a great integration with microwave sensors. The cross-section SEM image is presented in Fig. 24, which shows a well-controlled miniaturized channel cross section and the typical arch top of inkjet-printed microfluidic channels. Fig. 25(a) is an example of a fully inkjet-printed microfluidics sensor using a stepped impedance low-pass filter. The microfluidic channel is embedded beneath high-impedance segments to tune the impedance of the microstrip line, as illustrated in the inserted figure in Fig. 25(b). Therefore, the permittivity variation of the liquid inside the channel changes the attenuation of this filter, as shown in Fig. 25(b).

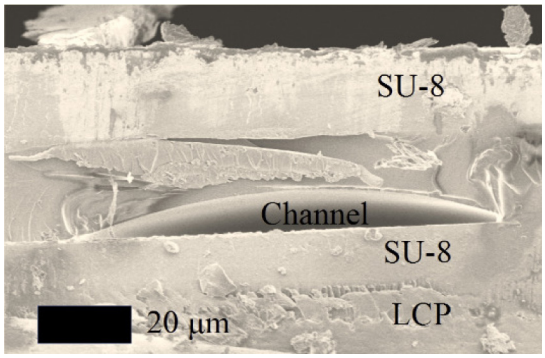

Fig. 24. *Cross-sectional SEM images of a proof-of-concept fully inkjet-printed microfluidic channel prototype [109].*

Inkjet-printing technology is excellent for microfluidic sensors, as it can accomplish both tasks of effectively realizing below 20-μm features, commonly required in microfluidic channels, while allowing metallization with

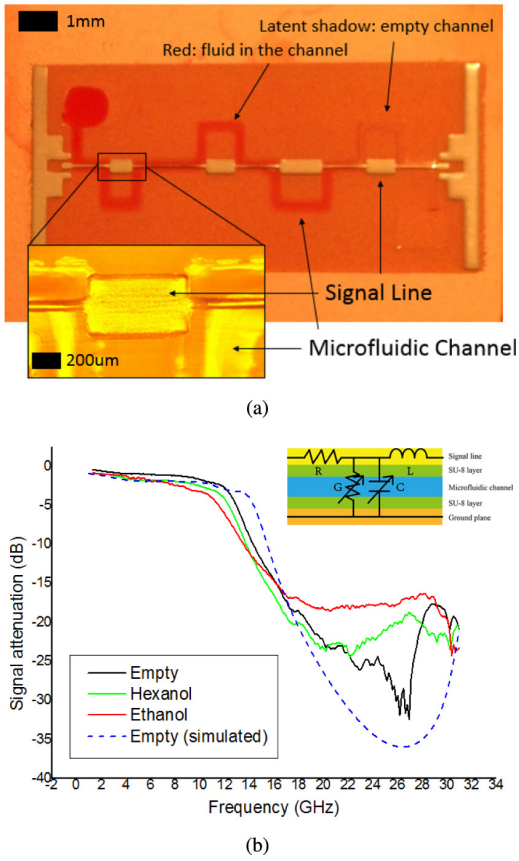

Fig. 25. *(a) Photo of a fully inkjet-printed low-pass filter-based microfluidics sensor prototype with an inserted magnified view of the zone within the rectangle. (b) Measured S21 of the sensor in (a) when different fluids are fed to the channel as well as for an empty channel along with the simulated attenuation for an empty channel with an inserted photo of the equivalent circuit of the cross section of the fully inkjet-printed liquid-reconfigurable microstrip line. The variable capacitance and conductance stems from the varying permittivity of the liquid inside the printed microfluidics channel [102].*

precise patterns using a single platform [16], [102], [109]. Moreover, inkjet-printing techniques are known for excellent flexibility and large-area scalability. Other AM techniques, such as 3-D printing and screen printing, also have been involved in fabricating microfluidic-based sensors and electronics [98], [99], [114], [115].

VI. CONCLUSION

In this paper, we have demonstrated various examples of additively manufactured RF components and topologies operating from the RFID up to the millimeter-wave frequency range. The recent explosion in interest for these technologies has triggered a rapid rise in the maturity and efficiency of AM tools and techniques, such as inkjet and 3-D printing, to the point of enabling their emerging industrial uses. As we have shown, this rise in maturity has provided a new framework within which the RF research community has been able to imagine and demonstrate entirely printed low-cost chipless motes, as well as all of the individual components required for the birth of low-cost and power-autonomous printed motes for the IoT and mm-wave 5G cellular networks, encompassing the complementary fields of energy harvesting and storage, backscattering communication front ends, passive RF components, interconnects, packages, shape-changing structures, and sensors. While it is true that AMTs have already made their entry in niche markets, as well as are demonstrating promising results in the packaging industry, we believe that the trends described in this paper, and exemplified by the reported state-of-the-art fully printed RF elements presented here, are early signs of a AM-enabled revolution in the RF and mmW landscape encompassing most state-of-the-art applications such as IoT, autonomous cars, and real-time biomonitoring wireless systems. ■

Acknowledgment

The authors would like to thank the National Science Foundation (NSF), Semiconductor Research Corporation (SRC), and the Defense Threat Reduction Agency (DTRA) for their support during this project.

REFERENCES

[1] W. S. Wong, M. L. Chabinyc, T.-N. Ng, and A. Salleo, "Materials and novel patterning methods for flexible electronics," in *Flexible Electronic*. New York, NY, USA: Springer-Verlag, 2009, pp. 143–181.

[2] L. Yang, A. Rida, R. Vyas, and M. M. Tentzeris, "RFID tag and RF structures on a paper substrate using inkjet-printing technology," *IEEE Trans. Microw. Theory Techn.*, vol. 55, no. 12, pp. 2894–2901, Dec. 2007.

[3] G. Orecchini, L. Yang, M. M. Tentzeris, and L. Roselli, "Wearable battery-free active paper-printed RFID tag with human-energy scavenger," in *IEEE MTT-S Int. Microw. Symp. Dig.*, Jun. 2011, p. 1.

[4] R. Parashkov, E. Becker, T. Riedl, H. H. Johannes, and W. Kowalsky, "Large area electronics using printing methods," *Proc. IEEE*, vol. 93, no. 7, pp. 1321–1329, Jul. 2005.

[5] B. Berman, "3-D printing: The new industrial revolution," *Bus. Horizons*, vol. 55, no. 2, pp. 155–162, 2012.

[6] J. van den Brand, R. Kusters, M. Barink, and A. Dietzel, "Flexible embedded circuitry: A novel process for high density, cost effective electronics," *Microelectron. Eng.*, vol. 87, no. 10, pp. 1861–1867, 2010.

[7] L. Yang, A. Rida, and M. M. Tentzeris, "Design and development of radio frequency identification (RFID) and RFID-enabled sensors on flexible low cost substrates," *Synthesis Lect. RF/Microw.*, vol. 1, no. 1, pp. 1–89, 2009.

[8] J. G. Hester *et al.*, "Additively manufactured nanotechnology and origami-enabled flexible microwave electronics," *Proc. IEEE*, vol. 103, no. 4, pp. 583–606, Apr. 2015.

[9] B. S. Cook and A. Shamim, "Inkjet printing of novel wideband and high gain antennas on low-cost paper substrate," *IEEE Trans. Antennas Propag.*, vol. 60, no. 9, pp. 4148–4156, Sep. 2012.

[10] B. S. Cook, B. Tehrani, J. R. Cooper, and M. M. Tentzeris, "Multilayer inkjet printing of millimeter-wave proximity-fed patch arrays on flexible substrates," *IEEE Antennas Wireless Propag. Lett.*, vol. 12, no. 10, pp. 1351–1354, Oct. 2013.

[11] B. S. Cook, J. R. Cooper, and M. M. Tentzeris, "Multi-layer RF capacitors on flexible substrates utilizing inkjet printed dielectric polymers," *IEEE Microw. Wireless Compon. Lett.*, vol. 23, no. 7, pp. 353–355, Jul. 2013.

[12] S. H. Ko, J. Chung, H. Pan, C. P. Grigoropoulos, and D. Poulikakos, "Fabrication of multilayer passive and active electric components on polymer using inkjet printing and low temperature laser processing," *Sens. Actuators A, Phys.*, vol. 134, no. 1, pp. 161–168, 2007.

[13] V. Subramanian, P. C. Chang, J. B. Lee, S. E. Molesa, and S. K. Volkman, "Printed organic transistors for ultra-low-cost RFID applications," *IEEE Trans. Compon. Packag. Technol.*, vol. 28, no. 4, pp. 742–747, Dec. 2005.

[14] M. S. Onses, E. Sutanto, P. M. Ferreira, A. G. Alleyne, and J. A. Rogers, "Mechanisms, capabilities, and applications of high-resolution electrohydrodynamic jet printing," *Small*, vol. 11, no. 34, pp. 4237–4266, Sep. 2015.

[15] B. K. Tehrani, C. Mariotti, B. S. Cook, L. Roselli, and M. M. Tentzeris, "Development, characterization, and processing of thin and thick inkjet-printed dielectric films," *Organ. Electron.*, vol. 29, pp. 135–141, Feb. 2016.

[16] W. Su, Q. Liu, B. Cook, and M. Tentzeris, "All-inkjet-printed microfluidics-based encodable flexible chipless RFID sensors," in *IEEE MTT-S Int. Microw. Symp. Dig.*, May 2016, pp. 1–4.

[17] L. Yang, R. Zhang, D. Staiculescu, C. P. Wong, and M. M. Tentzeris, "A novel conformal RFID-enabled module utilizing inkjet-printed antennas and carbon nanotubes for gas-detection applications," *IEEE Antennas Wireless Propag. Lett.*, vol. 8, pp. 653–656, 2009.

[18] M. M. Khan, F. A. Tahir, M. F. Farooqui, A. Shamim, and H. M. Cheema, "3.56-bitscm^2 compact inkjet printed and application specific chipless RFID tag," *IEEE Antennas Wireless Propag. Lett.*, vol. 15, pp. 1109–1112, 2016.

[19] R. Rezaiesarlak and M. Manteghi, "A space-frequency technique for chipless RFID tag localization," *IEEE Trans. Antennas Propag.*, vol. 62, no. 11, pp. 5790–5797, Nov. 2014.

[20] N. Zhang, M. Hu, L. Shao, and J. Yang, "Localization of printed chipless RFID in 3-D space," *IEEE Microw. Wireless Compon. Lett.*, vol. 26, no. 5, pp. 373–375, May 2016.

[21] J. G. D. Hester and M. M. Tentzeris, "Inkjet-printed flexible mm-wave Van-Atta reflectarrays: A solution for ultralong-range dense multitag and multisensing chipless RFID implementations for IoT smart skins," *IEEE Trans. Microw. Theory Techn.*, vol. 57, no. 5, pp. 1303–1309, May 2017.

[22] S. Shrestha, M. Balachandran, M. Agarwal, V. V. Phoha, and K. Varahramyan, "A chipless RFID sensor system for cyber centric monitoring applications," *IEEE Trans. Microw. Theory Techn.*, vol. 57, no. 5, pp. 1303–1309, May 2009.

[23] C. Mandel, B. Kubina, M. Schüßler, and R. Jakoby, "Passive chipless wireless sensor for two-dimensional displacement measurement," in *Proc. 41st Eur. Microw. Conf.*, Oct. 2011, pp. 79–82.

[24] D. Girbau, A. Ramos, A. Lazaro, S. Rima, and R. Villarino, "Passive wireless temperature sensor based on time-coded UWB chipless RFID tags," *IEEE Trans. Microw. Theory Techn.*, vol. 60, no. 11, pp. 3623–3632, Nov. 2012.

[25] E. M. Amin, M. S. Bhuiyan, N. C. Karmakar, and B. Winther-Jensen, "Development of a low cost printable chipless RFID humidity sensor," *IEEE Sensors J.*, vol. 14, no. 1, pp. 140–149, Jan. 2014.

[26] I. Preradovic, I. Balbin, N. C. Karmakar, and G. F. Swiegers, "Multiresonator-based chipless RFID system for low-cost item tracking," *IEEE Trans. Microw. Theory Techn.*, vol. 57, no. 5, pp. 1411–1419, May 2009.

[27] S. Preradovic and N. C. Karmakar, "Design of fully printable planar chipless RFID transponder with 35-bit data capacity," in *Proc. Eur. Microw. Conf.*, Oct. 2009, pp. 013–016.

[28] M. A. Islam and N. C. Karmakar, "A novel compact printable dual-polarized chipless RFID system," *IEEE Trans. Microw. Theory Techn.*, vol. 60, no. 7, pp. 2142–2151, Jul. 2012.

[29] D. Girbau, J. Lorenzo, and A. Lázaro,.C. Ferrater, and R. Villarino, "Frequency-coded chipless RFID tag based on dual-band resonators," *IEEE Antennas Wireless Propag. Lett.*, vol. 11, pp. 126–128, 2012.

[30] R. Nair, E. Perret, and S. Tedjini, "Temporal multi-frequency encoding technique for chipless RFID applications," in *IEEE MTT-S Int. Microw. Symp. Dig.*, Jun. 2012, pp. 1–3.

[31] K. Shibata, "Measurement of complex permittivity for liquid materials using the open-ended cut-off waveguide reflection method," in *Proc. China-Japan Joint Microw. Conf.*, Apr. 2011, pp. 1–4.

[32] T. N. D. Tibbits *et al.*, "New efficiency frontiers with wafer-bonded multi-junction solar cells," in *Proc. 29th Eur. Photovolt. Solar Energy Conf. Exhibit.*, Sep. 2014, pp. 1–4.

[33] K. Hwang *et al.*, "Toward large scale roll-to-roll production of fully printed perovskite solar cells," *Adv. Mater.*, vol. 27, no. 7, pp. 1241–1247, 2015.

[34] T. M. Eggenhuisen *et al.*, "High efficiency, fully inkjet printed organic solar cells with freedom of design," *J. Mater. Chem. A*, vol. 3, no. 14, pp. 7255–7262, 2015.

[35] M. Danesh and J. R. Long, "Photovoltaic antennas for autonomous wireless systems," *IEEE Trans. Circuits Syst. II, Exp. Briefs*, vol. 58, no. 12, pp. 807–811, Dec. 2011.

[36] A. Collado and A. Georgiadis, "Conformal hybrid solar and electromagnetic (EM) energy harvesting rectenna," *IEEE Trans. Circuits Syst. I, Reg. Papers*, vol. 60, no. 8, pp. 2225–2234, Aug. 2013.

[37] J. Bito, J. G. Hester, and M. M. Tentzeris, "Ambient RF energy harvesting from a two-way talk radio for flexible wearable wireless sensor devices utilizing inkjet printing technologies," *IEEE Trans. Microw. Theory Techn.*, vol. 63, no. 12, pp. 4533–4543, Dec. 2015.

[38] C. R. Valenta and G. D. Durgin, "Harvesting wireless power: Survey of energy-harvester conversion efficiency in far-field, wireless power transfer systems," *IEEE Microw. Mag.*, vol. 15, no. 4, pp. 108–120, Jun. 2014.

[39] J. Bito, B. Tehrani, B. Cook, and M. Tentzeris, "Fully inkjet-printed multilayer microstrip patch antenna for Ku-band applications," in *Proc. IEEE Antennas Propag. Soc. Int. Symp.*, Jul. 2014, pp. 854–855.

[40] B. S. Cook, J. R. Cooper, and M. M. Tentzeris, "Multi-layer RF capacitors on flexible substrates utilizing inkjet printed dielectric polymers," *IEEE Microw. Compon. Lett.*, vol. 23, no. 7, pp. 353–355, Jul. 2013.

[41] B. S. Cook *et al.*, "Inkjet-printed, vertically-integrated, high-performance inductors and transformers on flexible LCP substrate," in *IEEE MTT-S Int. Microw. Symp. Dig.*, Tampa, FL, USA, Jun. 2014, pp. 1–4.

[42] N. Sani *et al.*, "All-printed diode operating at 1.6 GHz," *Proc. Nat. Acad. Sci. USA*, vol. 111, no. 33, pp. 11943–11948, 2014.

[43] P. Sharma and T. S. Bhatti, "A review on electrochemical double-layer capacitors," *Energy Conv. Manage.*, vol. 51, no. 12, pp. 2901–2912, Dec. 2010.

[44] P. Chen, H. Chen, J. Qiu, and C. Zhou, "Inkjet printing of single-walled carbon nanotube/RuO_2 nanowire supercapacitors on cloth fabrics and flexible substrates," *Nano Res.*, vol. 3, no. 8, pp. 594–603, Jul. 2010.

[45] J. D. MacKenzie and C. Ho, "Perspectives on energy storage for flexible electronic systems," *Proc. IEEE*, vol. 103, no. 4, pp. 535–553, Apr. 2015.

[46] Y. P. Zhang and D. Liu, "Antenna-on-chip and antenna-in-package solutions to highly integrated millimeter-wave devices for wireless communications," *IEEE Trans. Antennas Propag.*, vol. 57, no. 10, pp. 2830–2841, Oct. 2009.

[47] A. Jentzsch and W. Heinrich, "Theory and measurements of flip-chip interconnects for frequencies up to 100 GHz," *IEEE Trans. Microw. Theory Techn.*, vol. 49, no. 5, pp. 871–878, May 2001.

[48] S. A. Nauroze, J. Hester, W. Su, and M. M. Tentzeris, "Inkjet-printed substrate integrated waveguides (SIW) with 'drill-less' vias on paper substrates," in *IEEE MTT-S Int. Microw. Symp. Dig.*, May 2016, pp. 1–4.

[49] T. Falat, J. Felba, A. Moscicki, and J. Borecki, "Nano-silver inkjet printed interconnections through the microvias for flexible electronics," in *Proc. 11th IEEE Conf. Nanotechnol. (IEEE-NANO)*, Aug. 2011, pp. 473–477.

[50] T. Kawase, H. Sirringhaus, R. H. Friend, and T. Shimoda, "Inkjet printed via-hole interconnections and resistors for all-polymer transistor circuits," *Adv. Mater.*, vol. 13, no. 21, p. 1601, 2001.

[51] G. McKerricher, J. Gonzalez, and A. Shamim, "All inkjet printed 3D microwave capacitors and inductors with vias," in *IEEE MTT-S Int. Microw. Symp. Dig.*, Jun. 2013, pp. 1–3.

[52] S. Kim, A. Shamim, A. Georgiadis, H. Aubert, and M. M. Tentzeris, "Fabrication of fully inkjet-printed vias and SIW structures on thick polymer substrates," *IEEE Trans. Compon. Packag. Manuf. Technol.*, vol. 6, no. 3, pp. 486–496, Mar. 2016.

[53] B. K. Tehrani, B. S. Cook, and M. M. Tentzeris, "Inkjet-printed 3D interconnects for millimeter-wave system-on-package solutions," in *IEEE MTT-S Int. Microw. Symp. Dig.*, May 2016, pp. 1–4.

[54] U. R. Pfeiffer *et al.*, "A chip-scale packaging technology for 60-GHz wireless chipsets," *IEEE Trans. Microw. Theory Techn.*, vol. 54, no. 8, pp. 3387–3397, Aug. 2006.

[55] C. Mariotti, L. Aluigi, T. T. Thai, F. Alimenti, L. Roselli, and M. M. Tentzeris, "A fully inkjet-printed 3D transformer balun for conformal and rollable microwave applications," in *Proc. IEEE Antennas Propag. Soc. Int. Symp.*, Jul. 2014, pp. 330–331.

[56] C. Mariotti, B. S. Cook, L. Roselli, and M. M. Tentzeris, "State-of-the-art inkjet-printed metal-insulator-metal (MIM) capacitors on silicon substrate," *IEEE Microw. Wireless Compon. Lett.*, vol. 25, no. 1, pp. 13–15, Jan. 2015.

[57] R. E. Taylor, C. M. Boyce, M. C. Boyce, and B. L. Pruitt, "Planar patterned stretchable electrode arrays based on flexible printed circuits," *J. Micromech. Microeng.*, vol. 23, no. 10, p. 105004, 2013.

[58] A. Hirsch, H. O. Michaud, A. P. Gerratt, S. De Mulatier, and S. P. Lacour, "Intrinsically stretchable biphasic (solid–liquid) thin metal films," *Adv. Mater.*, vol. 28, no. 22, pp. 4507–4512, Feb. 2016.

[59] Z. Li *et al.*, "Rational design of a printable, highly conductive silicone-based electrically conductive adhesive for stretchable radio-frequency antennas," *Adv. Funct. Mater.*, vol. 25, no. 3, pp. 464–470, 2015.

[60] T. Le, "Nano-material based flexible radio frequency sensors for wearable health and environment monitoring: Designs and prototypes utilizing 3D/inkjet printing technologies," Ph.D. dissertation, Georgia Inst. Technol., Atlanta, GA, USA, 2016.

[61] C. Mias, "Varactor-tunable frequency selective surface with resistive-lumped-element biasing grids," *IEEE Microw. Wireless Compon. Lett.*, vol. 15, no. 9, pp. 570–572, Sep. 2005.

[62] B. Schoenlinner, A. Abbaspour-Tamijani, L. C. Kempel, and G. M. Rebeiz, "Switchable low-loss RF MEMS Ka-band frequency-selective surface," *IEEE Trans. Microw. Theory Techn.*, vol. 52, no. 11, pp. 2474–2481, Nov. 2004.

[63] M. Li, B. Yu, and N. Behdad, "Liquid-tunable frequency selective surfaces," *IEEE Microw. Wireless Compon. Lett.*, vol. 20, no. 8, pp. 423–425, Aug. 2010.

[64] A. C. Dec. Lima, E. A. Parker, and R. J. Langley, "Tunable frequency selective surface using liquid substrates," *Electron. Lett.*, vol. 30, no. 4, pp. 281–282, Feb. 1994.

[65] J. A. Bossard *et al.*, "Tunable frequency selective surfaces and negative-zero-positive index metamaterials based on liquid crystals," *IEEE Trans. Antennas Propag.*, vol. 56, no. 5, pp. 1308–1320, May 2008.

[66] T. K. Chang, R. J. Langley, and E. A. Parker, "Frequency selective surfaces on biased ferrite substrates," *Electron. Lett.*, vol. 30, no. 15, pp. 1193–1194, Jul. 1994.

[67] Z. Y. Wei, Z. V. Guo, L. Dudte, H. Y. Liang, and L. Mahadevan, "Geometric mechanics of periodic pleated origami," *Phys. Rev. Lett.*, vol. 110, p. 215501, May 2013.

[68] X. Liu, S. Yao, S. V. Georgakopoulos, B. S. Cook, and M. M. Tentzeris, "Reconfigurable helical antenna based on an origami structure for wireless communication system," in *IEEE MTT-S Int. Microw. Symp. Dig.*, Jun. 2014, pp. 1–4.

[69] W. D. Reynolds, S. K. Jeon, J. A. Banik, and T. W. Murphey, "Advanced folding approaches for deployable spacecraft payloads," in *ASME Int. Design Eng. Tech. Conf. Comput. Inf. Eng. Conf.*, 2013, p. V06BT07A043.

[70] K. Kuribayashi *et al.*, "Self-deployable *origami* stent grafts as a biomedical application of Ni-rich TiNi shape memory alloy foil," *Mater. Sci. Eng., A*, vol. 419, no. 1, pp. 131–137, 2006.

[71] A. P. Thrall and C. P. Quaglia, "Accordion shelters: A historical review of origami-like deployable shelters developed by the US military," *Eng. Struct.*, vol. 59, pp. 686–692, Feb. 2014.

[72] M. Nogi, N. Komoda, K. Otsuka, and K. Suganuma, "Foldable nanopaper antennas for origami electronics," *Nanoscince*, vol. 5, no. 10, pp. 4395–4399, 2013.

[73] K. Skucha, Z. Fan, K. Jeon, A. Javey, and B. Boser, "Palladium/silicon nanowire Schottky barrier-based hydrogen sensors," *Sens. Actuators B, Chem.*, vol. 145, no. 1, pp. 232–238, 2010.

[74] H. J. Yoon *et al.*, "Carbon dioxide gas sensor using a graphene sheet," *Sens. Actuators B, Chem.*, vol. 157, no. 1, pp. 310–313, 2011.

[75] J. Jang, J. Ha, and J. Cho, "Fabrication of water-dispersible polyaniline-poly(4-styrenesulfonate) nanoparticles for inkjet-printed chemical-sensor applications," *Adv. Mater.*, vol. 19, no. 13, pp. 1772–1775, 2007.

[76] P. Qi *et al.*, "Toward large arrays of multiplex functionalized carbon nanotube sensors for highly sensitive and selective molecular detection," *Nano Lett.*, vol. 3, no. 3, pp. 347–351, 2003.

[77] C. Bittencourt *et al.*, "WO3 films modified with functionalised multi-wall carbon nanotubes: Morphological, compositional and gas response studies," *Sens. Actuators B, Chem.*, vol. 115, no. 1, pp. 33–41, 2006.

[78] Y. Lu *et al.*, "Room temperature methane detection using palladium loaded single-walled carbon nanotube sensors," *Chem. Phys. Lett.*, vol. 391, nos. 4–6, pp. 344–348, Jun. 2004.

[79] J. P. Novak, E. S. Snow, E. J. Houser, D. Park, J. L. Stepnowski, and R. A. McGill, "Nerve agent detection using networks of single-walled carbon nanotubes," *Appl. Phys. Lett.*, vol. 83, no. 19, pp. 4026–4028, 2003.

[80] J. Li, Y. Lu, Q. Ye, M. Cinke, J. Han, and M. Meyyappan, "Carbon nanotube sensors for gas and organic vapor detection," *Nano Lett.*, vol. 3, no. 7, pp. 929–933, 2003.

[81] J. R. Stetter and J. Li, "Amperometric gas sensors a review," *Chem. Rev.*, vol. 108, no. 2, pp. 352–366, 2008.

[82] J. Fouletier, "Gas analysis with potentiometric sensors. A review," *Sens. Actuators*, vol. 3, pp. 295–314, Jan. 1983.

[83] J. R. Stetter, E. F. Stetter, D. Ebeling, M. Findlay, and V. Patel, "Printed gas sensor," U.S. Patent 12953672 Nov. 24, 2010.

[84] K. Wallgren and S. Sotiropoulos, "Oxygen sensors based on a new design concept for amperometric solid state devices," *Sens. Actuators B, Chem.*, vol. 60, nos. 2–3, pp. 174–183, 1999.

[85] Y. Jung *et al.*, "Fully printed flexible and disposable wireless cyclic voltammetry tag," *Sci. Rep.*, vol. 5, Jan. 2015.

[86] W. H. Brattain and J. Bardeen, "Surface properties of germanium," *Bell Syst. Tech. J.*, vol. 32, no. 1, pp. 1–41, Jan. 1953.

[87] C. Occhiuzzi, A. Rida, G. Marrocco, and M. Tentzeris, "RFID passive gas sensor integrating carbon nanotubes," *IEEE Trans. Microw. Theory Techn.*, vol. 59, no. 10, pp. 2674–2684, Oct. 2011.

[88] Y. Ling *et al.*, "A printable CNT-based FM passive wireless sensor tag on a flexible substrate with enhanced sensitivity," *IEEE Sensors J.*, vol. 14, no. 4, pp. 1193–1197, Apr. 2014.

[89] R. S. Nair, E. Perret, S. Tedjini, and T. Baron, "A group-delay-based chipless RFID humidity tag sensor using silicon nanowires," *IEEE Antennas Wireless Propag. Lett.*, vol. 12, pp. 729–732, 2013.

[90] J. G. D. Hester, M. M. Tentzeris, and Y. Fang, "UHF lumped element model of a fully-inkjet-printed single-wall-carbon-nanotube-based inter-digitated electrodes breath sensor," in *Proc. IEEE Antennas Propag. Soc. Int. Symp. (APSURSI)*, Jun. 2016, pp. 1959–1960.

[91] J. G. D. Hester, M. M. Tentzeris, and Y. Fang, "Inkjet-printed, flexible, high performance, carbon nanomaterial based sensors for ammonia and DMMP gas detection," in *Proc. Eur. Microw. Conf.*, Sep. 2015, pp. 857–860.

[92] G. M. Whitesides, "The origins and the future of microfluidics," *Nature*, vol. 442, no. 27, pp. 368–373, Jul. 2006.

[93] C. Mariotti, W. Su, B. S. Cook, L. Roselli, and M. M. Tentzeris, "Development of low cost, wireless, inkjet printed microfluidic RF systems and devices for sensing or tunable electronics," *IEEE Sensors J.*, vol. 15, no. 6, pp. 3156–3163, Jun. 2015.

[94] K. Entesari and A. P. Saghati, "Fluidics in microwave components," *IEEE Microw. Mag.*, vol. 17, no. 6, pp. 50–75, Jun. 2016.

[95] W. Su, C. Mariotti, B. Cook, S. Lim, L. Roselli, and M. Tentzeris, "A metamaterial-inspired temperature stable inkjet-printed microfluidic-tunable bandstop filter," in *Proc. 44th Eur. Microw. Conf.*, Oct. 2014, pp. 9–12.

[96] W. Su, B. Cook, and M. M. Tentzeris, "A low-cost inkjet-printed microfluidics-based tunable loop antenna feed by microfluidics-based tunable balun," in *Proc. 9th Eur. Conf. Antennas Propag.*, Lisbon, Portugal, Apr. 2015, pp. 1–2.

[97] W. Su, B. Cook, M. Tentzeris, C. Mariotti, and L. Roselli, "A novel inkjet-printed microfluidic tunable coplanar patch antenna," in *Proc. IEEE Antennas Propag. Soc. Int. Symp.*, Jul. 2014, pp. 858–859.

[98] W. Su, R. Bahr, S. A. Nauroze, and M. M. Tentzeris, "3D printed reconfigurable helical antenna based on microfluidics and liquid metal alloy," in *Proc. IEEE Antennas Propag. Soc. Int. Symp.*, Jul. 2016, pp. 1–2.

[99] S. Moscato *et al.*, "Exploiting 3D printed substrate for microfluidic SIW sensor," in *Proc. Eur. Microw. Conf.*, Sep. 2015, pp. 28–31.

[100] W. Su, B. S. Cook, and M. M. Tentzeris, "Additively manufactured microfluidics-based 'Peel-and-replace' RF sensors for wearable applications," *IEEE Trans. Microw. Theory Techn.*, vol. 64, no. 6, pp. 1928–1936, Jun. 2016.

[101] W. Su, J. Cooper, B. Cook, M. Tentzeris, C. Mariotti, and L. Roselli, "Inkjet-printed dual microfluidic-based sensor integrated system," in *Proc. IEEE SENSORS*, Nov. 2015, pp. 1–3.

[102] W. Su, B. S. Cook, J. R. Cooper, and M. M. Tentzeris, "Low-cost flexible all-inkjet-printed microfluidic sensor," in *Proc. 19th Int. Conf. Miniaturized Syst. Chem. Life Sci.*, 2015, pp. 1–3.

[103] Y. Hao and R. Foster, "Wireless body sensor networks for health-monitoring applications," *Physiol. Meas.*, vol. 29, no. 11, p. R27, 2008.

[104] D. R. Reyes, D. Iossifidis, P.-A. Auroux, and A. Manz, "Micro total analysis systems. 1. Introduction, theory, and technology," *Anal. Chem.*, vol. 74, no. 12, pp. 2623–2636, 2002.

[105] F. Benito-Lopez, S. Coyle, R. Byrne, and D. Diamond, "Sensing sweat in real-time using wearable microfluidics," in *Proc. 7th Int. Workshop Wearable Implantable Body Sens. Netw.*, Singapore, Jun. 2010.

[106] P. Petong, R. Pottel, and U. Kaatze, "Dielectric relaxation of h-bonded liquids. Mixtures of ethanol and n-hexanol at different compositions and temperatures," *J. Phys. Chem. A*, vol. 103, no. 31, pp. 6114–6121, 1999.

[107] R. R. Nigmatullin, M. A.-G. Jafar, N. Shinyashiki, S. Sudo, and S. Yagihara, "Recognition of a new permittivity function for glycerol by the use of the eigen-coordinates method," *J. Non-Crystalline Solids*, vol. 305, pp. 96–111, Jul. 2002. [Online]. Available: http://www.sciencedirect.com/science/article/pii/S0022309302011250

[108] A. Tidar *et al.*, "Microwave dielectric relaxation study of 1-hexanol with 1-propenol mixture by using time domain reflectometry at 300K," in *Proc. Appl. Electromagn. Conf.*, Dec. 2009, pp. 1–4.

[109] W. Su, B. S. Cook, Y. Fang, and M. M. Tentzeris, "Fully inkjet-printed microfluidics: A solution to low-cost rapid three-dimensional microfluidics fabrication with numerous electrical and sensing applications," *Sci. Rep.*, vol. 6, p. 6, Oct. 2016.

[110] G. M. Whitesides and A. D. Stroock, "Flexible methods for microfluidics," *Phys. Today*, vol. 54, no. 6, pp. 42–48, 2001.

[111] D. C. Duffy, J. C. McDonald, O. J. Schueller, and G. M. Whitesides, "Rapid prototyping of microfluidic systems in poly (dimethylsiloxane)," *Anal. Chem.*, vol. 70, no. 23, pp. 4974–4984, Dec. 1998.

[112] A. Ebrahimi, W. Withayachumnankul, S. Al-Sarawi, and D. Abbott, "High-sensitivity metamaterial-inspired sensor for microfluidic dielectric characterization," *IEEE Sensors J.*, vol. 14, no. 5, pp. 1345–1351, May 2014.

[113] K. Abe, K. Suzuki, and D. Citterio, "Inkjet-printed microfluidic multianalyte chemical sensing paper," *Anal. Chem.*, vol. 80, no. 18, pp. 6928–6934, 2008.

[114] J. L. Erkal *et al.*, "3D printed microfluidic devices with integrated versatile and reusable electrodes," *Lab Chip*, vol. 14, no. 12, pp. 2023–2032, 2014.

[115] G. Jenkins *et al.*, "Printed electronics integrated with paper-based microfluidics: New methodologies for next-generation health care," *Microfluidics Nanofluidics*, vol. 19, no. 2, pp. 251–261, Oct. 2015.

ABOUT THE AUTHORS

Syed Abdullah Nauroze (Student Member, IEEE) received the B.Sc. degree (honors) in computer engineering from the University of Engineering and Technology, Taxila, Pakistan, in 2005 and the M.Sc. degree in electrical engineering from Royal Institute of Technology (KTH), Stockholm, Sweden, in 2008. Currently, he is working toward the Ph.D. degree in electrical and computer engineering at Georgia Institute of Technology, Atlanta, GA, USA.

During 2008–2009, he worked at Microsystems Technology Laboratory, KTH, where he conducted research on on-chip millimeter-wave antennas for automotive radar and future wireless applications. Currently, he is a Research Assistant at the Agile Technologies for High-performance Electromagnetic Novel Applications (ATHENA) lab, Georgia Institute of Technology. He has a teaching experience of seven years. His research interests include application of AM techniques like 3-D printing and inkjet printing for flexible and origami-based RF structures.

Mr. Nauroze is a recipient of a prestigious Swedish Institute scholarship in 2006 and the Fulbright Scholarship in 2014 for his M.S. and Ph.D. degrees, respectively.

Jimmy G. Hester (Student Member, IEEE) spent two intense preparation years studying fundamental chemistry, math, and physics, after which he was admitted in INP Toulouse, ENSEEIHT, Toulouse, France, where he received a graduate degree and the M.S. degree in electrical and signal processing engineering, majoring in radio-frequency electronics, in 2012 and 2014, respectively. He received the M.S. in electrical and computer engineering from Georgia Institute of Technology, Atlanta, GA, USA, in 2014, where he is currently working toward the Ph.D. degree in electrical and computer engineering.

He is a Research Assistant in the Agile Technologies for High-performance Electromagnetic Novel Applications (ATHENA) group, Georgia Institute of Technology. His research interests lie at the interface between radio-frequency engineering and material science, in the form of flexible electronics technologies and nanotechnologies. Recently, he has been working toward the use of carbon nanomaterials applied to inkjet-printed RF sensing components for flexible low-cost ubiquitous gas sensing applications. His work covers the entire development process, from the development of inkjet inks, improvement of fabrication methods, sensor component design, high-frequency characterization and environmental testing to the design, simulation, and fabrication of the RF system embedding the sensor.

Bijan K. Tehrani (Student Member, IEEE) received the B.S. and M.S. degrees in electrical engineering from Georgia Institute of Technology, Atlanta, GA, USA, in 2013 and 2015, respectively, where he is currently working toward the Ph.D. degree in electrical and computer engineering, where he is supervised by Prof. M. M. Tentzeris in the Agile Technologies for High-performance Electromagnetic Novel Applications (ATHENA) research lab.

His research interests include the development of advanced multilayer inkjet-printing fabrication processes for the realization of additive, postprocessed millimeter-wave antenna integration with system-on-chip and system-in-package solutions.

Wenjing Su (Student Member, IEEE) was born in Hunan, China, in 1991. She received the B.S. degree in electrical engineering from Beijing Institute of Technology, Beijing, China, in 2013. She is currently working toward the Ph.D. degree in electrical and computer engineering at Georgia Institute of Technology, Atlanta, GA, USA.

In fall 2013, she joined the Agile Technologies for High-performance Electromagnetic Novel Applications (ATHENA) research group, led by Dr. M. M. Tentzeris and has been working as a Graduate Research Assistant. Her research interfaces the microfluidics and microwave, and focuses on additively manufactured (inkjet/3-D-printed) microfluidics sensors for Internet of Things (IoT) and Lab-on-Chip (LoC) applications as well as tunable antennas and passive RF components for wideband/reconfigurable communication systems.

Jo Bito (Student Member, IEEE) received the B.S. degree in electrical and electronic engineering from Okayama University, Okayama, Japan, in 2013. From 2010 to 2011, he joined the international programs in engineering (IPENG), and studied at University of Illinois Urbana-Champaign, Champaign, IL, USA. He received the M.S. degree in electrical and computer engineering from Georgia Institute of Technology, Atlanta, GA, USA, in 2016, where he is now working toward the Ph.D. degree.

He is a Research Assistant in the Agile Technologies for High-performance Electromagnetic Novel Applications (ATHENA) group, Georgia Institute of Technology. His research interests include the application of inkjet-printing technology for flexible and wearable electronics, RF energy harvesting, and wireless power transfer systems.

Mr. Bito was a recipient of the Japan Student Services Organization (JASSO) Long Term Scholarship beginning in 2013.

Ryan Bahr (Student Member, IEEE) received the B.S. and M.S. degrees in electrical engineering from Georgia Institute of Technology, Atlanta, GA, USA, where he is currently working toward the Ph.D. degree in electrical and computer engineering, supervised by Prof. M. M. Tentzeris.

His research focuses on applying 3-D-printing techniques for millimeter-wave and packaging applications utilizing new materials.

John Kimionis (Student Member, IEEE) received the Diploma degree and the M.Sc. degree in electronic and computer engineering from the Technical University of Crete, Chania, Greece, in 2011 and 2013, respectively. He is currently working toward the Ph.D. degree at the School of Electrical and Computer Engineering, Georgia Institute of Technology, Atlanta, GA, USA.

He is a Research Assistant with the Agile Technologies for High-performance Electromagnetic Novel Applications (ATHENA) group, Georgia Institute of Technology. His research interests are in the areas of spectral-efficient and energy-efficient backscatter radio and RFID, software-defined radio for sensor networks, RF front-end design for wireless sensors, and AM techniques.

Mr. Kimionis has received fellowship awards for his undergraduate and graduate studies, and he is a Texas Instruments Scholar for his mentoring service in the Opportunity Research Scholars (ORS) program at Georgia Tech. He has received IEEE student travel grants, and was the recipient of the First Best Student Paper Award at the 2014 IEEE International Conference on RFID-Technologies and Applications (RFID-TA), Tampere, Finland, as well as the Second Best Student Paper Award at the 2011 IEEE International Conference on RFID-Technologies and Applications (RFID-TA), Sitges, Barcelona, Spain. He is a member of the IEEE Microwave Theory and Techniques Society, the IEEE Communications Society, and a board member of the IEEE MTT-24 RFID Technologies Committee.

Manos M. Tentzeris (Fellow, IEEE) received the Diploma degree (*magna cum laude*) in electrical and computer engineering from the National Technical University of Athens, Athens, Greece and the M.S. and Ph.D. degrees in electrical engineering and computer science from the University of Michigan, Ann Arbor, MI, USA.

He is currently Ken Byers Professor in Flexible Electronics with the School of Electrical and Computer Engineering, Georgia Institute of Technology (Georgia Tech), Atlanta, GA, USA. He has published more than 600 papers in refereed journals and conference proceedings, five books, and 25 book chapters. He has helped develop academic programs in highly integrated/multilayer packaging for RF and wireless applications using ceramic and organic flexible materials, paper-based RFIDs and sensors, biosensors, wearable electronics, 3-D/4-D/inkjet-printed electronics, "green" electronics, energy harvesting and wireless power transfer systems, NFC systems, nanotechnology applications in RF, origami-folded electromagnetics, microwave MEMs, SOP-integrated (UWB, multiband, mmW, conformal) antennas and heads the Agile Technologies for High-performance Electromagnetic Novel Applications (ATHENA) research group (20 researchers) at Georgia Tech. He has served as the Head of the GT-ECE Electromagnetics Technical Interest Group, as the Georgia Electronic Design Center Associate Director for RFID/Sensors research from 2006 to 2010, and as the Georgia Tech NSF-Packaging Research Center Associate Director for RF Research and the RF Alliance Leader from 2003 to 2006. He was a Visiting Professor at the Technical University of Munich, Munich, Germany, during summer 2002; a Visiting Professor at GTRI-Ireland, Athlone, Ireland, during summer 2009; and a Visiting Professor at LAAS-CNRS, Toulouse, France, during summer 2010. He has given more than 100 invited talks at various universities and companies all over the world.

Dr. Tentzeris was the recipient/corecipient of the 2016 Bell Labs Prize Third Award, the 2015 IET Microwaves, Antennas and Propagation Premium Award, the 2014 Georgia Tech ECE Distinguished Faculty Achievement Award, the 2014 IEEE RFID-TA Best Student Paper Award, the 2013 IET Microwaves, Antennas and Propagation Premium Award, the 2012 FiDiPro Award in Finland, the iCMG Architecture Award of Excellence, the 2010 IEEE Antennas and Propagation Society Piergiorgio L. E. Uslenghi Letters Prize Paper Award, the 2011 International Workshop on Structural Health Monitoring Best Student Paper Award, the 2010 Georgia Tech Senior Faculty Outstanding Undergraduate Research Mentor Award, the 2009 IEEE Transactions on Components and Packaging Technologies Best Paper Award, the 2009 E.T.S.Walton Award from the Irish Science Foundation, the 2007 IEEE APS Symposium Best Student Paper Award, the 2007 IEEE IMS Third Best Student Paper Award, the 2007 ISAP 2007 Poster Presentation Award, the 2006 IEEE MTT Outstanding Young Engineer Award, the 2006 Asian-Pacific Microwave Conference Award, the 2004 IEEE Transactions on Advanced Packaging Commendable Paper Award, the 2003 NASA Godfrey "Art" Anzic Collaborative Distinguished Publication Award, the 2003 IBC International Educator of the Year Award, the 2003 IEEE CPMT Outstanding Young Engineer Award, the 2002 International Conference on Microwave and Millimeter-Wave Technology Best Paper Award (Beijing, CHINA), the 2002 Georgia Tech-ECE Outstanding Junior Faculty Award, the 2001 ACES Conference Best Paper Award and the 2000 NSF CAREER Award, and the 1997 Best Paper Award of the International Hybrid Microelectronics and Packaging Society. He was the TPC Chair for IEEE IMS 2008 Symposium and the Chair of the 2005 IEEE CEM-TD Workshop and he is the Vice-Chair of the RF Technical Committee (TC16) of the IEEE CPMT Society. He is the founder and chair of the RFID Technical Committee (TC24) of the IEEE MTT Society and the Secretary/Treasurer of the IEEE C-RFID. He is the Associate Editor of the IEEE Transactions on Microwave Theory and Techniques, the IEEE Transactions on Advanced Packaging, and the *International Journal on Antennas and Propagation*. He is a member of URSI-Commission D, a member of MTT-15 committee, an Associate Member of EuMA, a Fellow of the Electromagnetic Academy, and a member of the Technical Chamber of Greece. He served as one of the IEEE MTT-S Distinguished Microwave Lecturers from 2010 to 2012, and he is currently serving as the IEEE C-RFID Distinguished Lecturer.